# Energetic Neutral Atoms Around Extrasolar Planets

M. Holmström<sup>1</sup>, A. Ekenbäck<sup>1</sup>, F. Selsis<sup>2</sup>, T. Penz<sup>3</sup>, H. Lammer<sup>4</sup> and P.Wurz<sup>5</sup>

- 1. Swedish Institute of Space Physics, Kiruna, Sweden
- 2. Centre de Recherche en Astrophysique de Lyon (CRAL) and École Normale Supérieure (ENS), Lyon, France,
- 3. Istituto Nazionale di Astrofisica, Osservatorio Astronomico di Palermo Giuseppe S. Vaiata, Palermo, Italy,
- 4. Space Research Institute, Austrian Academy of Sciences, Graz, Austria,
- 5. University of Bern, Switzerland

IRF Seminar October 4, 2007

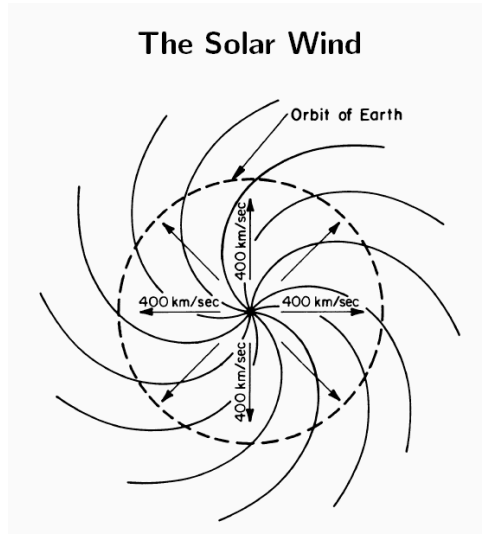


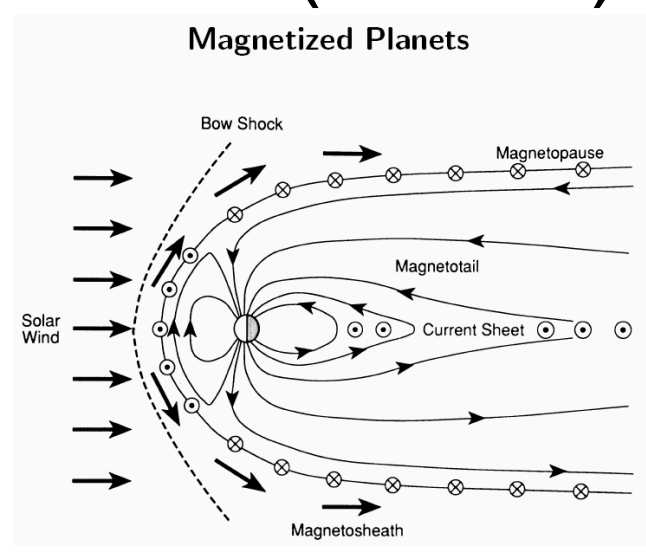
matsh@irf.se
www.irf.se/~matsh/

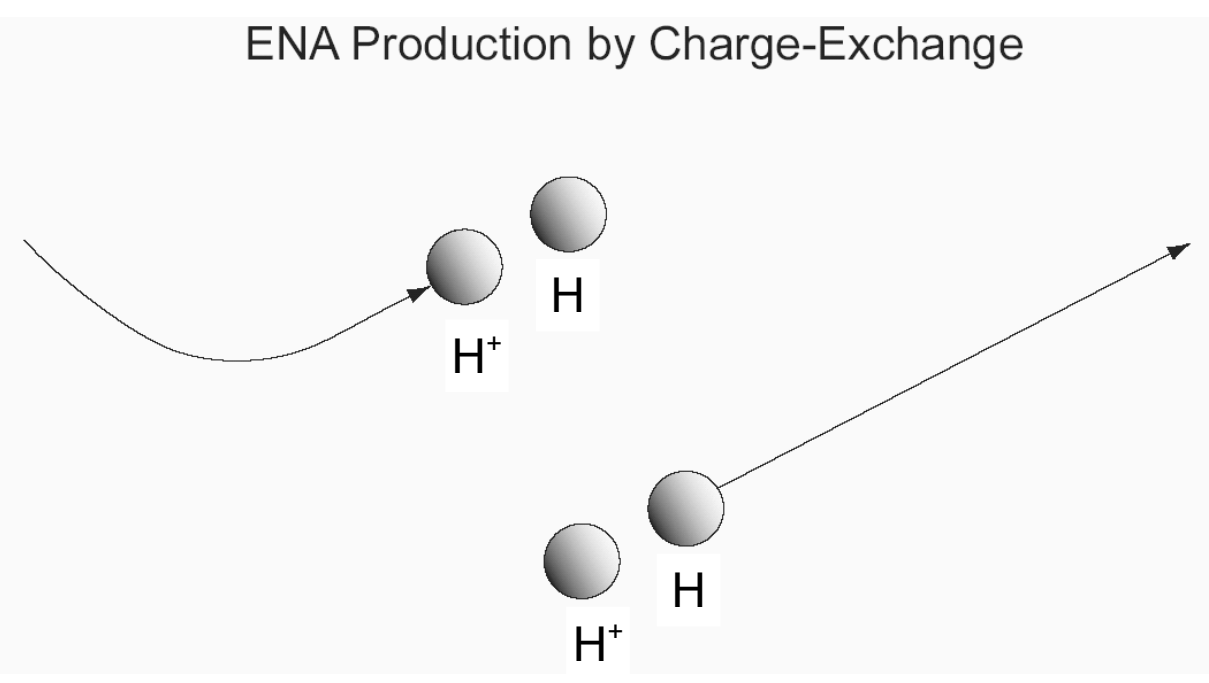
#### Overview

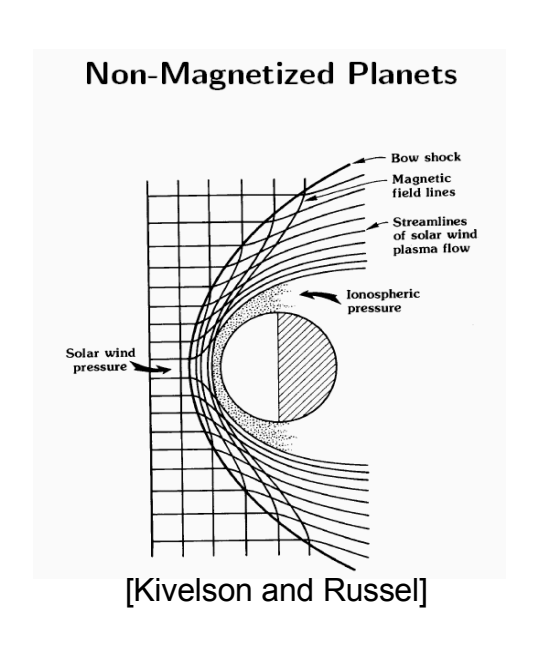
- Energetic neutral atoms (ENAs)
- Extrasolar planets
- The Hubble observation of H around HD 209458b
- Model of ENA production at HD 209458b
- Comparison of model results and observations
- Stellar wind estimates

# Energetic Neutral Atoms (ENAs)







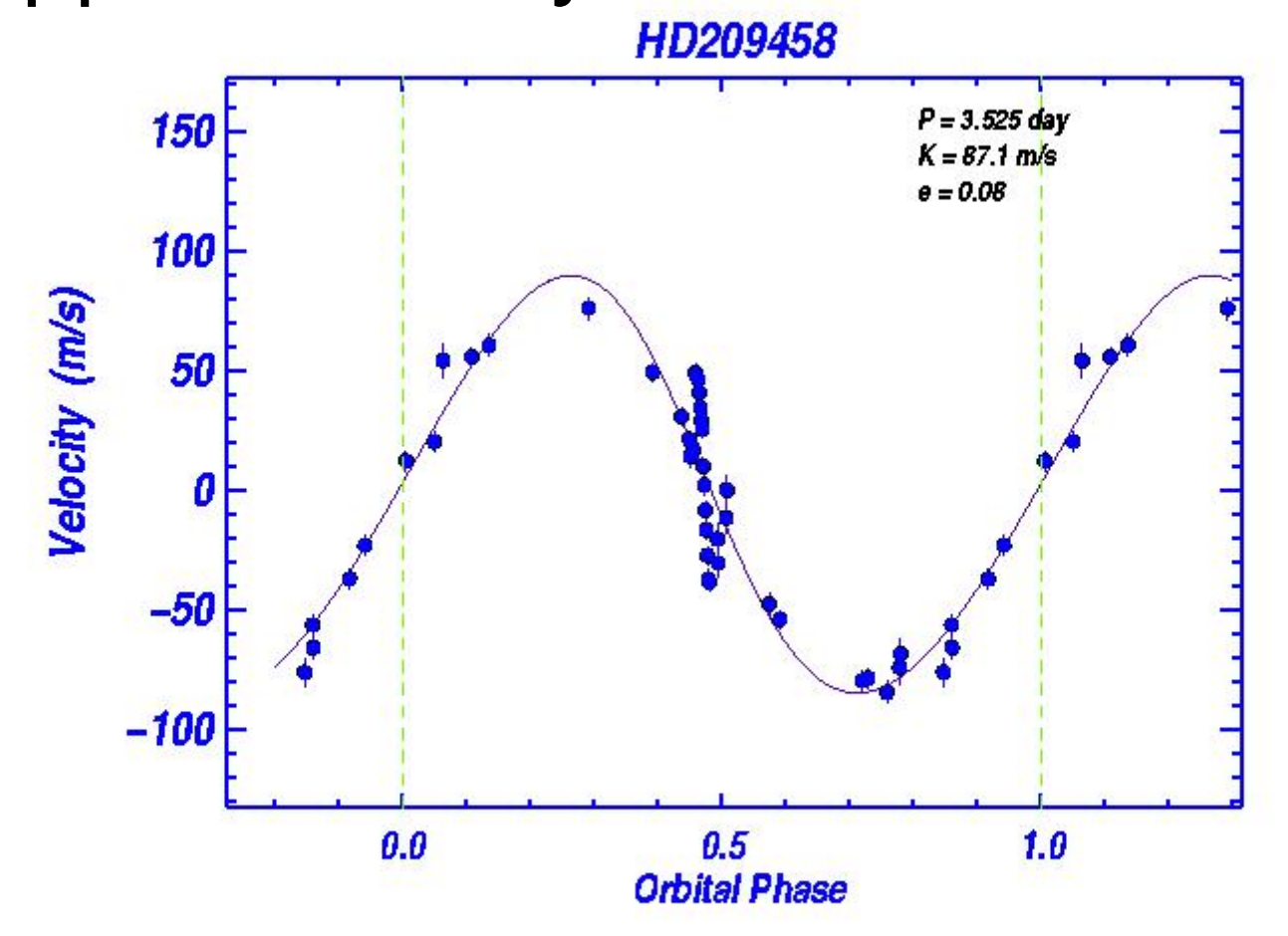


#### **ENA Observations in the Solar System**

ENAs from charge-exchange between solar wind protons and exospheric hydrogen has been observed at all planets where suitable ENA detectors were present:

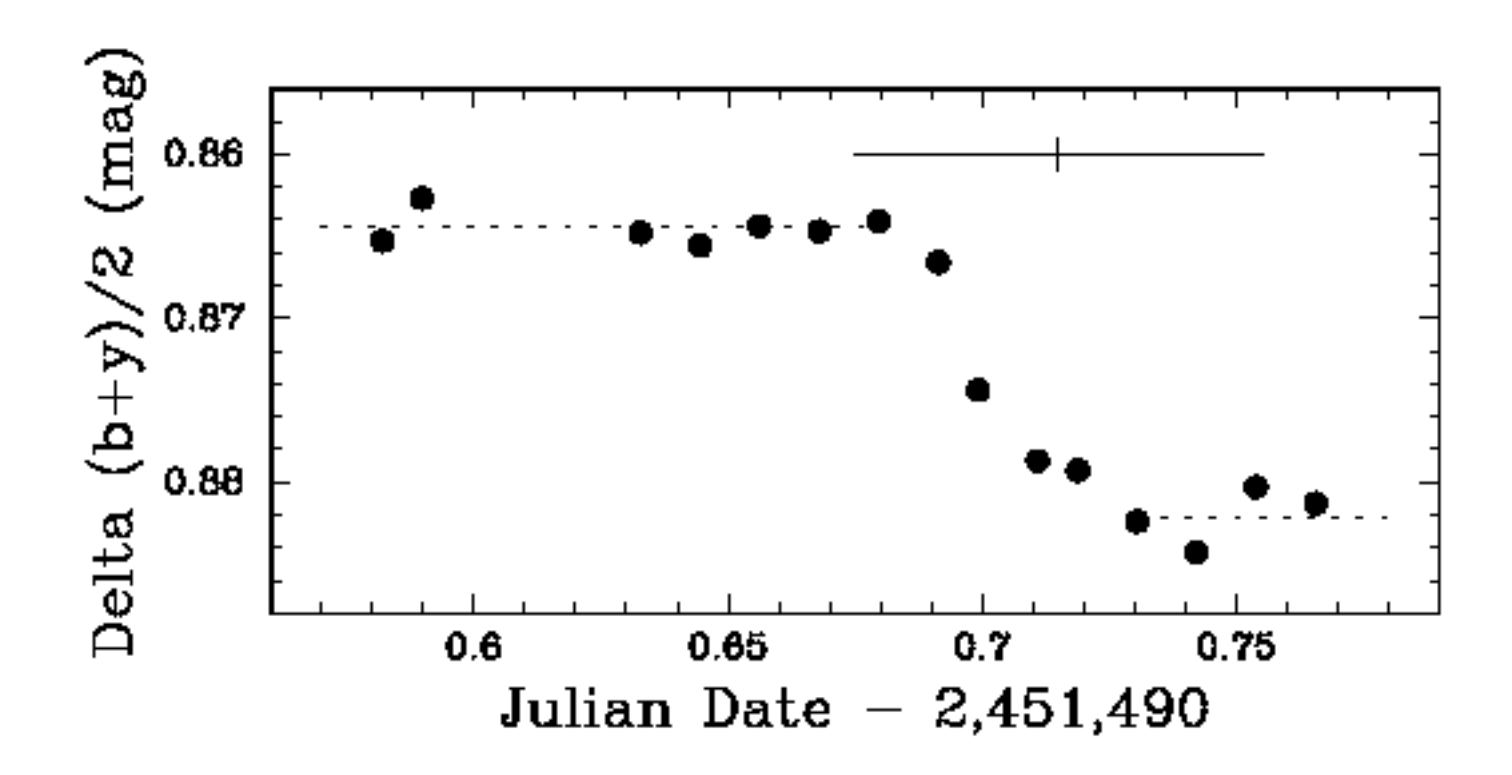
- At Earth by IMAGE
- At Mars by Mars Express
- At Venus by Venus Express

#### Doppler Velocity Curve for HD 209458



HD209458 velocity curve with the Keplerian orbital fit for a period P=3.52 days. Error bars are shown. The derived companion mass is: M sin i = 0.63 Jupiter Masses. The transit ensures that the orbital inclination, i, is nearly 90 deg. So the companion mass is 0.63 Jupiter masses. The odd behavior in the velocities near phase=0.5 is due to the rotation of the star, as the planet blocks of the approaching and receding limbs of the star.

# HD 209458 Planetary Transit



Photometric observations of HD 209458 from the night of 1999 Nov. 7 UT taken with the T8 0.80m APT

at Fairborn Observatory showing ingress of the planetary transit.

The measured transit depth is 0.017 mag or 1.58%.

The error bar shows the predicted time of mid transit and its uncertainty computed from the Keck radial velocities.

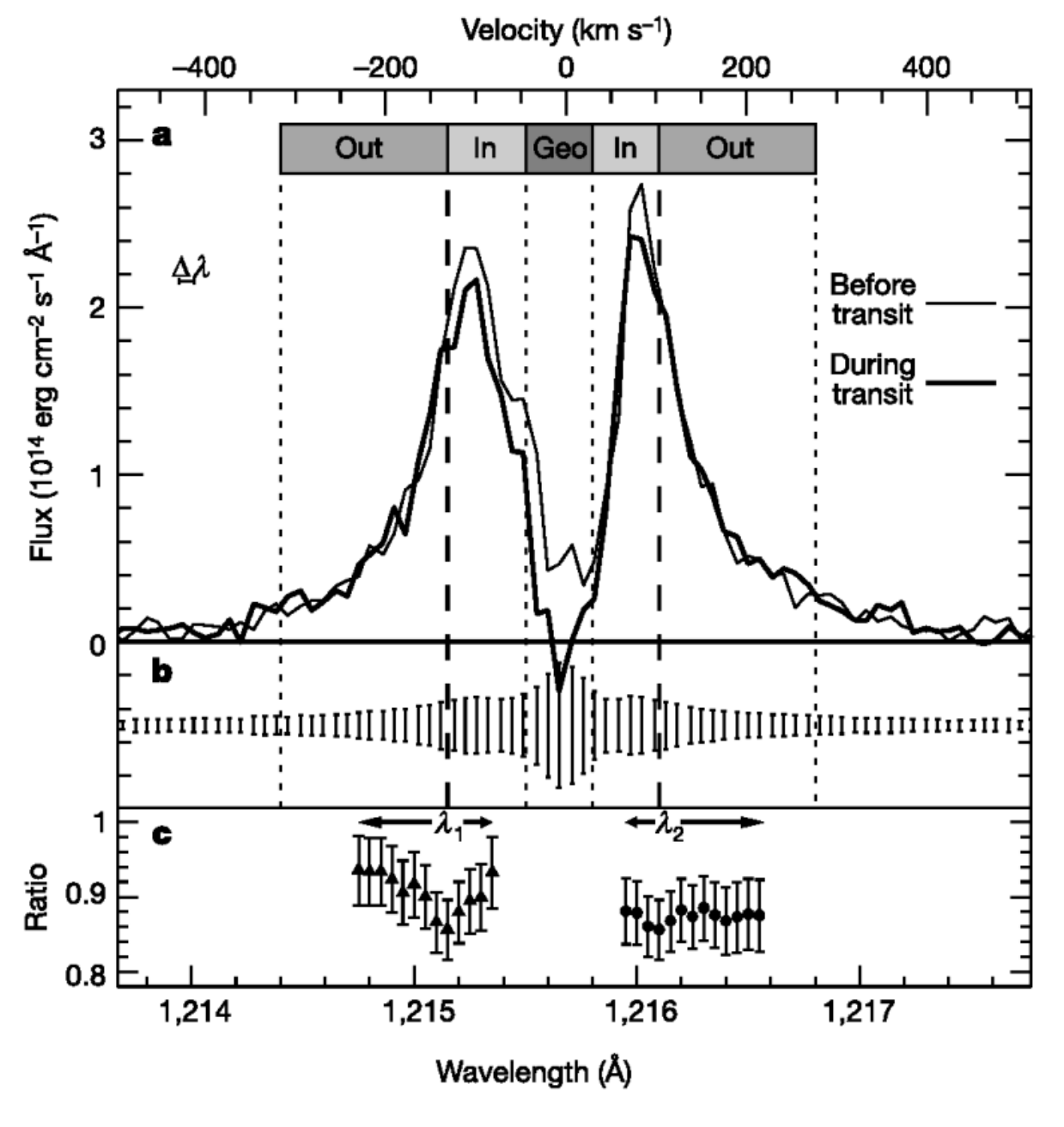


**Figure 2** The HD209458 Lyman  $\alpha$  profile observed with the G140M grating.

Vidal-Madjar, Nature, 422, 2003

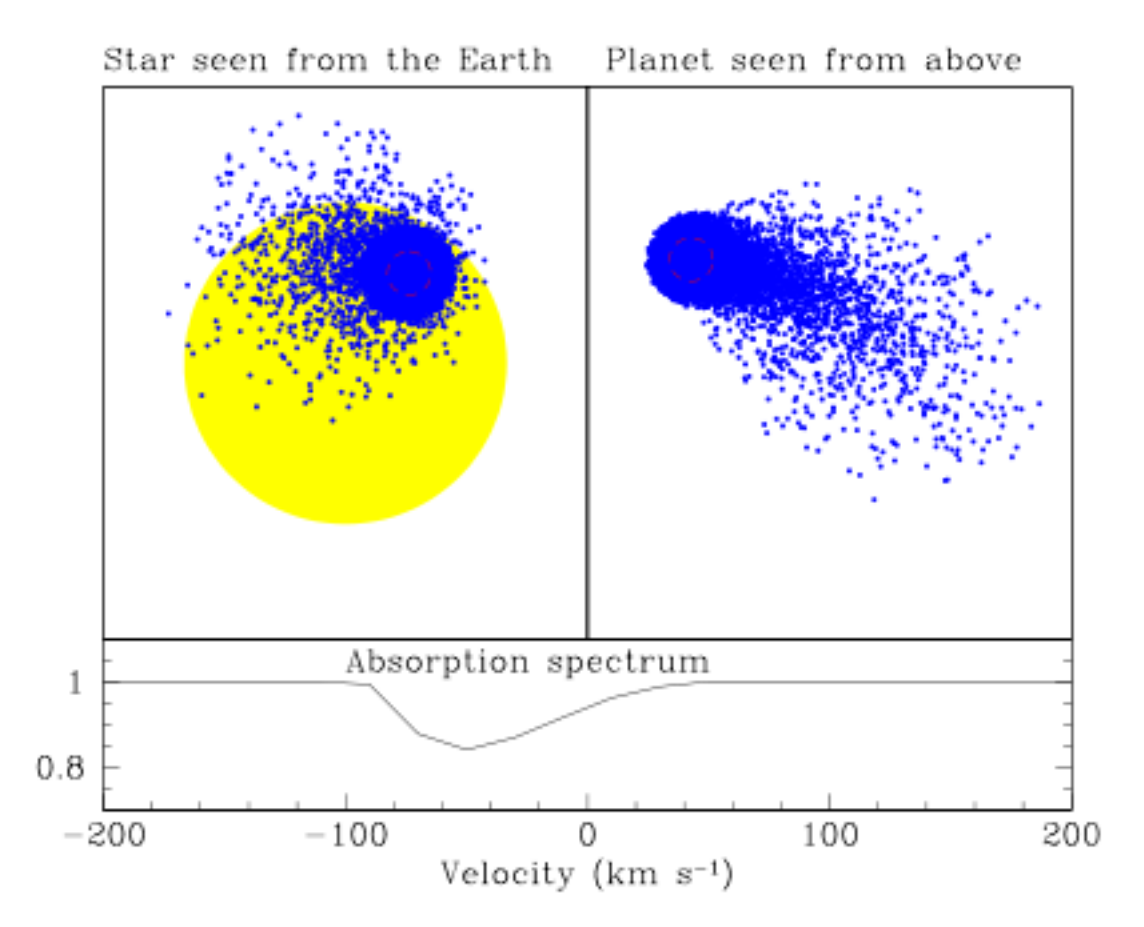
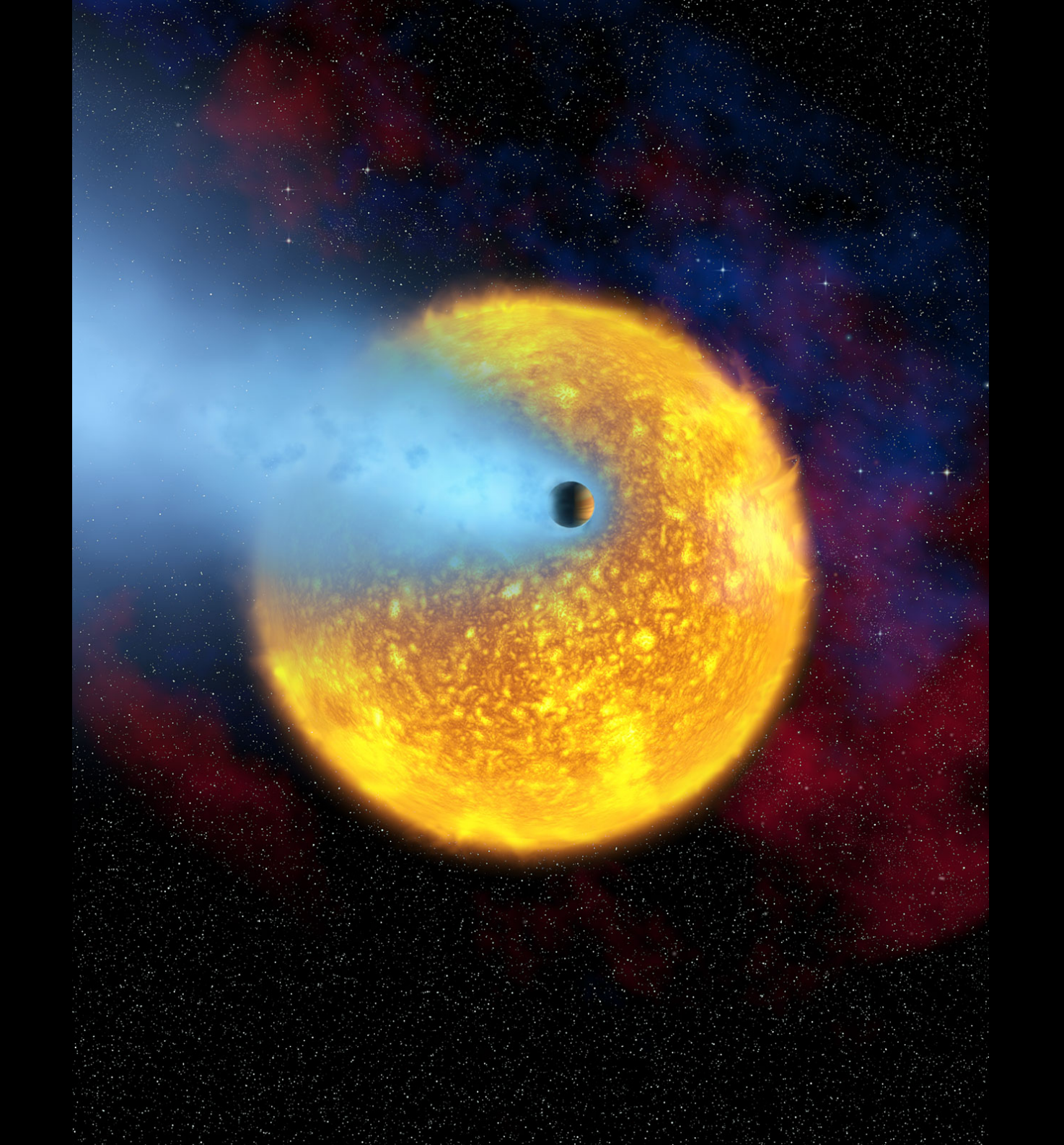


Figure 3. A numerical simulation of hydrogen atoms sensitive to radiation pressure (0.7 times the stellar gravitation) above an altitude of 0.5 times the Roche radius where the density is assumed to be  $2\times10^5$  cm<sup>-3</sup> is presented here. It corresponds to an escape flux of  $\sim10^{10}$  g s<sup>-1</sup>. The mean ionization lifetime of escaping hydrogen atoms is 4 hours. The model yields an atom population in a curved cometary like tail.

Vidal-Madjar, A. & Lecavelier des Etangs, A., "Osiris" (HD209458b), an evaporating planet, in *Extrasolar Planets: Today and Tomorrow*, ASP Conference Proceedings, Vol. 321. Edited by J.-P. Beaulieu, A. Lecavelier des Etangs, & C. Terguem, 152- (2004). ISBN: 1-58381-183-4



#### **ICARUS**

#### Aeronomy of extra-solar giant planets at small orbital distances

#### Roger V. Yelle

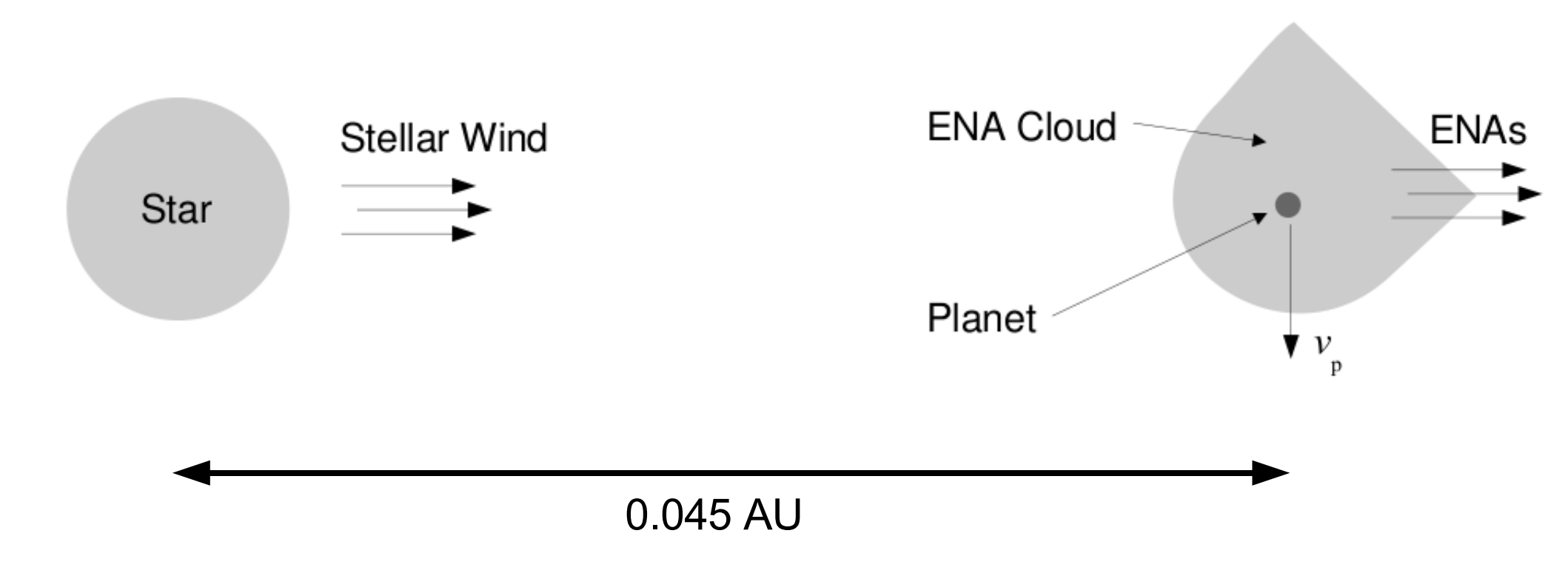
There is a qualitative agreement between the hot thermospheres calculated here and the HLyα absorption measurements of Vidal-Madjar et al. (2003). The observed absorption signature has a magnitude of  $\sim 15\%$ . In the visible, the planet occults about 1% of the star light, so an absorption of 15% implies that H is optically thick to about  $4R_P$ . The reference model has an H density of  $4.1 \times 10^5$  cm<sup>-3</sup> at  $3R_P$ and a temperature of 10,909 K, implying a tangential column abundance of  $1.7 \times 10^{16}$  cm<sup>-2</sup>. Assuming a Maxwell-Boltzmann distribution for the H cloud and using the temperature quoted above implies an absorption cross section at Ly $\alpha$  line center of 5.6  $\times$  10<sup>-14</sup> cm<sup>2</sup> and an optical depth of ~ 1000. Thus, the H distribution calculated here is opaque out to several planetary radii, in rough agreement with the measurements. Vidal-Madjar et al. (2003) also show that the absorption extends roughly 0.5 Å from the center of the Ly $\alpha$ 

line. This only occurs if the H distribution is characterized by a high temperature. Assuming a Maxwell–Boltzmann distribution and a temperature of 10,000 K implies a Doppler broadened absorption line with a width of 0.055 Å. An optical depth at line center of 1000 implies that optical depth unity is reached roughly 3 Doppler widths from line center or at 0.16 Å. This is of the same order but somewhat smaller than measured by Vidal-Madjar et al. (2003).

A more quantitative comparison requires improvements to the models. As mentioned earlier, the assumptions contained in these aeronomical models become questionable at a distance of  $3R_P$  from the planet. The gravitation field of the central star and radiation pressure can no longer be neglected and a 1D calculation is no longer possible. Instead it is preferable to construct kinetic models that calculate the H distribution by integrating along trajectories in the exosphere.

# Can Energetic Neutral Atoms (ENAs) Explain the Observation?

# Illustration of the geometry



Planet centered coordinate system. x-axis is planet-star line

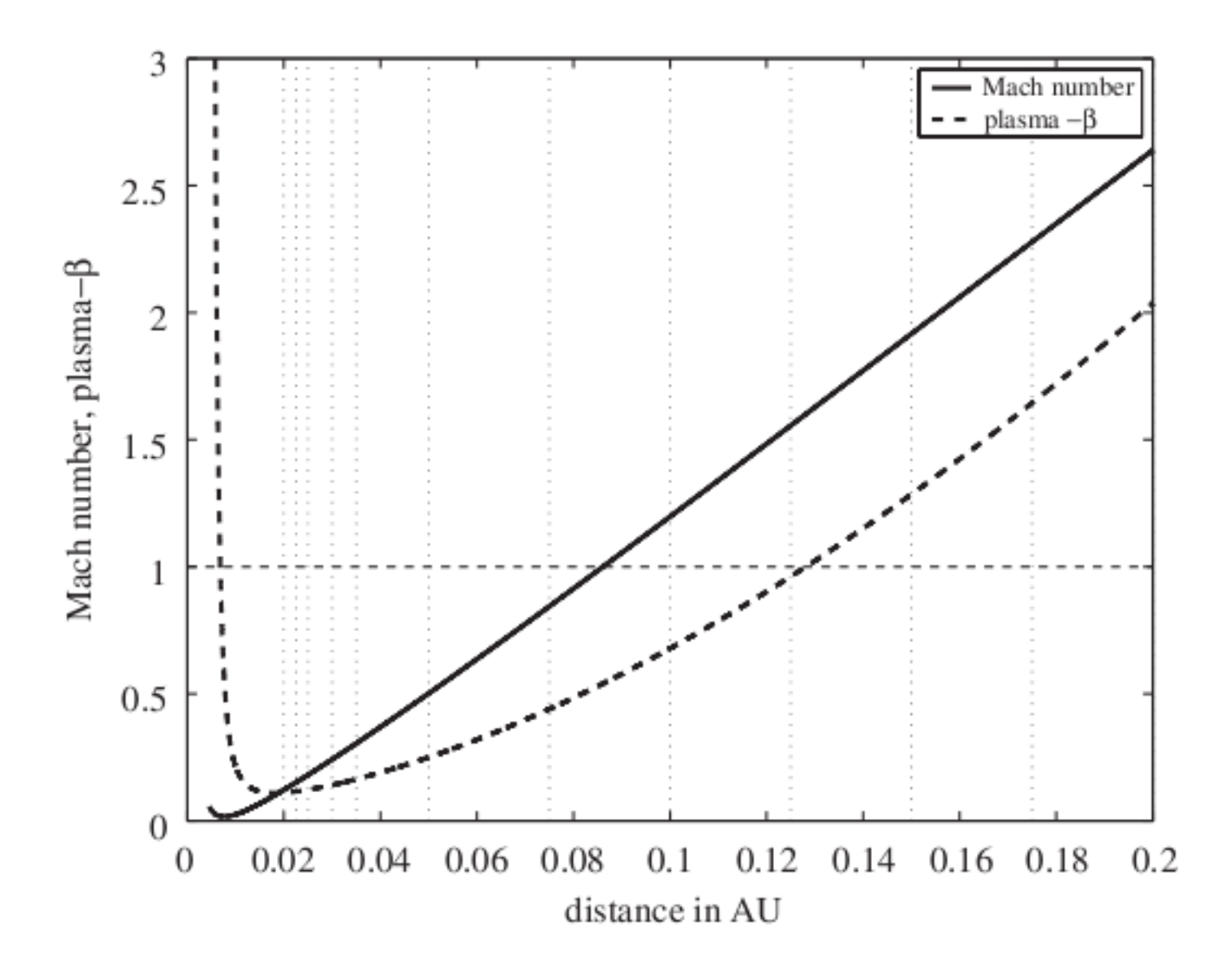
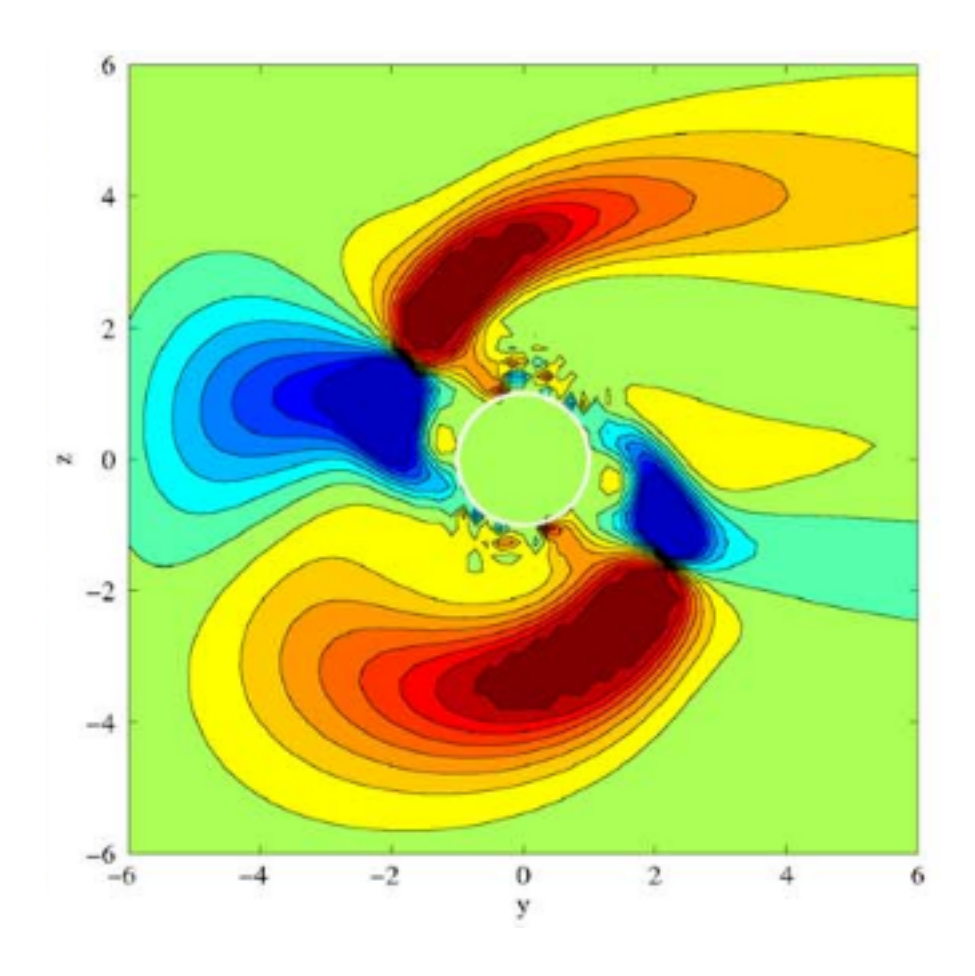
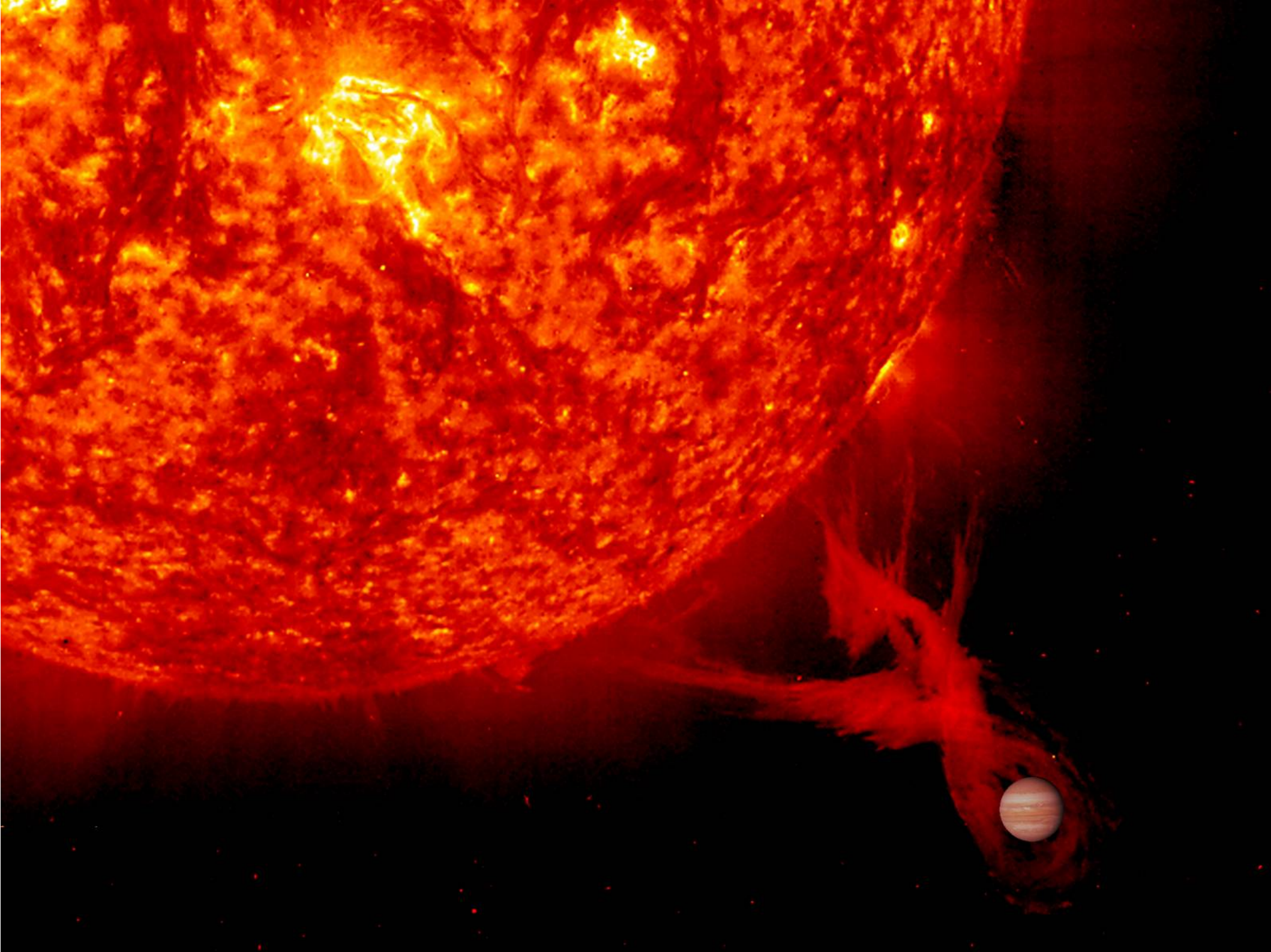


Fig. 7. Alfvén Mach number (solid line) and plasma- $\beta$  (dashed line) of the stellar wind model in dependance of the distance in AU from the star. The locations of the simulated planets are marked with dotted lines.





#### A model of the ENA production at HD 209458b

- Hydrogen atoms launched from an inner boundary
- Stellar wind protons inflowing
- Charge-exchange outside an obstacle
- Forces on an H atom:
  - gravity (planet), coriolis force (stellar)
- Events for an H atom:
  - charge exchange with a proton (ENA production)
  - elastic collision with another H atom
  - photon collision (radiation pressure)
  - photoionization

The outer boundary of the simulation domain is the box  $x_{\min} \le x \le x_{\max}$ ,  $y_{\min} \le y \le y_{\max}$ , and  $z_{\min} \le z \le z_{\max}$ . The inner boundary is a sphere of radius  $R_0$ .

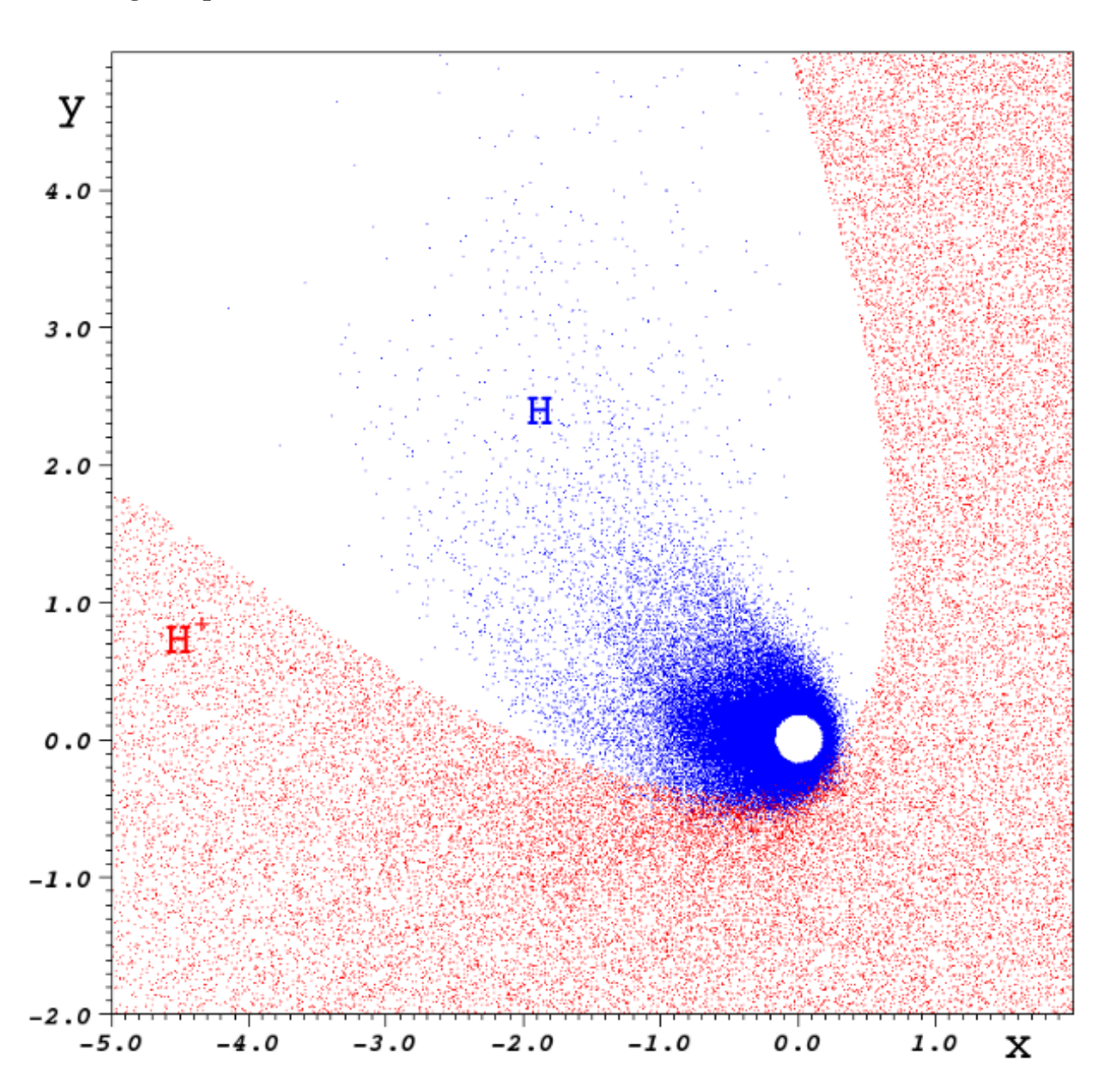
At the start of the simulation the domain is empty of particles. Then hydrogen meta-particles are launched from the inner boundary at a rate of 600 meta-particles per second. Each metaparticles corresponds to  $N_m$  hydrogen atoms. The location on the inner boundary of each launched particle is randomly drawn with probability proportional to the local hydrogen exobase density. The velocity of each launched particle is randomly drawn from a probability distribution proportional to

$$(\mathbf{n} \cdot \mathbf{v}) e^{-a|\mathbf{v}|^2},$$

where n is the local unit surface normal, v is the velocity of the particle, and a = m/(2kT), m is the mass of a neutral, k is Boltzmann's constant, and T is the temperature (at the exobase position). Note that the distribution used is not a Maxwellian, but the distribution of the flux through a surface (the exobase) given a Maxwellian distribution at the location<sup>1</sup>. The number flux through the surface is  $n/\sqrt{4\pi a}$ , where n is the inner boundary hydrogen density, for a total production rate of  $nR_0^2\sqrt{8\pi kT/m}$  s<sup>-1</sup>. After an hydrogen atom is launched from the inner boundary, we numerically integrate its trajectory with a time step of 25 seconds.

Before each time step we also fill the x-axis shadow cells (cells just outside the simulation domain) with proton meta-particles of the same weight as for hydrogen,  $N_m$ . After each time step the shadow cells and the obstacle region are emptied of protons. The protons are drawn from a Maxwellian distribution with temperature  $T_{\rm sw}$  and bulk velocity  $v_{\rm rel}$ . The relative velocity at the planet,  $v_{\rm rel}$ , is related to the stellar wind velocity and the planet's orbital velocity by  $v_{\rm rel}^2 = v_{\rm SW}^2 + v_{\rm p}^2$ . This ensures that a uniform stellar wind eventually builds up in the simulation domain, outside the obstacle. The boundary conditions in the y- and z-directions are periodic.

# x-y plane slice around z=0



Between time steps, the following events can occur for an exospheric atom

- Collision with an UV photon. Following Hodges² this occurs as an absorption of the photon (Δv opposite the sun direction) followed by isotropic reradiation (Δv in a random direction). From Hodges² we use a velocity change Δv = 3.27 m/s. The collision rate used τ<sub>r</sub>, is a scaled Earth value and the rate is zero if the particle is in the shadow behind the planet. This collision rate and velocity change correspond to a 2.3 m/s² acceleration of an hydrogen atom due to radiation pressure.
- Photoionization by a solar photon occurs at a rate of τ<sub>i</sub> when an exospheric hydrogen atom is outside the optical shadow behind the planet, and then the meta-particle is removed from the simulation.
- Charge exchange with a stellar wind proton. If the hydrogen atom is outside the obstacle it can charge exchange with a solar wind proton, producing an ENA. This is done using the DSMC method described in the next section. We define the obstacle by the conic surface (X, ρ) such that X = -ρ/(20R<sub>p</sub>) + X<sub>0</sub> where R<sub>p</sub> is the planet's radius, and X<sub>0</sub> is the obstacle stand off distance. Here ρ is the distance to the planet-star line, aberrated by an angle of arctan(v<sub>p</sub>/v<sub>sw</sub>) to account for the finite stellar wind speed relative to the planet's orbital speed. The shape of the obstacle is clearly seen in Fig. 1 that shows the protons and hydrogen atoms in a slice through the simulation domain.
- Elastic collision with another hydrogen atom, according to the DSMC method described in the next section.

For the radiation pressure and photoionization event rates,  $\tau$ , after each time step, for each metaparticle, we draw a random time from an exponential distribution with mean  $\tau$ , and the event occur
if this time is smaller than the time step. Note that we only consider ENAs produced outside the
obstacle, so the fluxes presented here is a lower bound. Additional ENAs are produced inside, but
including those would require a complete ion flow model.

The forces acting on a hydrogen atom is planetary gravity and the Coriolis force from the coordinate system rotating at an angular rate of  $\omega$ . The values of physical constants and parameters used in the simulation are listed in Table 1. Values of numerical parameters can be found in Table 2. The distribution of protons and hydrogen atoms in the simulation domain is illustrated in Figure 1. The total number of meta-particles at the final time is approximately  $2 \cdot 10^6$ , of which  $1.5 \cdot 10^5$  are ENAs.

#### Collisions

The collisions between hydrogen atoms are modeled using the direct simulation Monte Carlo (DSMC) method<sup>3</sup>, where we divide the computational domain into cells. Then after each time step the particles that are in the same cells are concidered for hard sphere collisions. From Bird<sup>3</sup> (Eq. 1.6), the frequency of collisions experienced by a single particle is  $\nu = n\overline{\sigma}v_r$ , where n is the total number density of all species,  $\sigma$  is the total collisional crossection, and  $v_r$  is the relative velocity between the particle and the particles in the surrounding gas. The bar denotes average. From this we get that the total collision frequency in a volume is

$$\frac{1}{2}n\nu = \frac{1}{2}n^2\overline{\sigma v_r} \tag{1}$$

For a each pair of particles, their collision probability is proportional to  $\sigma v_r$ . For a cell, we estimate n by  $N_c N_m/V_c$  where  $N_c$  is the number of particles in the cell,  $N_m$  is the number of particles per meta-particle, and  $V_c$  is the cell volume. If  $N_m$  is different for different particles, we must sum all  $N_m$  instead of using  $N_c N_m$ .

To avoid an operation count proportional to  $N_c^2$ , following Garcia<sup>1</sup> (p. 359), we do not directly compute the averages. Instead we estimate a maximum value of  $\sigma v_r$ ,  $(\sigma v_r)_{max}$ , and use that in (1) to compute the number of trials. For each trial we then draw a random pair, and a random number R on  $[0, (\sigma v_r)_{max}]$ . If  $\sigma v_r > R$  for the chosen pair, the collision is accepted.

The random pair above is uniformly distributed if  $N_m$  is the same for all particles, as is the case for these simulations.

#### Time integration

To avoid energy dissipation, the time advance of the particles from time t to time  $t + \Delta t$ , is done using the symplectic integrators derived by Candy and Rozmus<sup>4</sup>,

$$\mathbf{x} \leftarrow \mathbf{x} + c_k \Delta t \mathbf{v},$$
 $\mathbf{a} \leftarrow \mathbf{a}(\mathbf{x}, t),$ 
 $\mathbf{v} \leftarrow \mathbf{v} + d_k \Delta t \mathbf{a},$ 
 $t \leftarrow t + c_k \Delta t,$ 
(2)

for k = 1, ...n. Here x are the particle positions, v the velocities, and  $\mathbf{a}(\mathbf{x}, t)$  the accelerations. The coefficients  $c_k$  and  $d_k$  can be found in Candy<sup>4</sup>. The global order of accuracy is n, and n = 2 corresponds to the Leapfrog method. In this work we have used n = 4.

#### Some Constants and Parameters

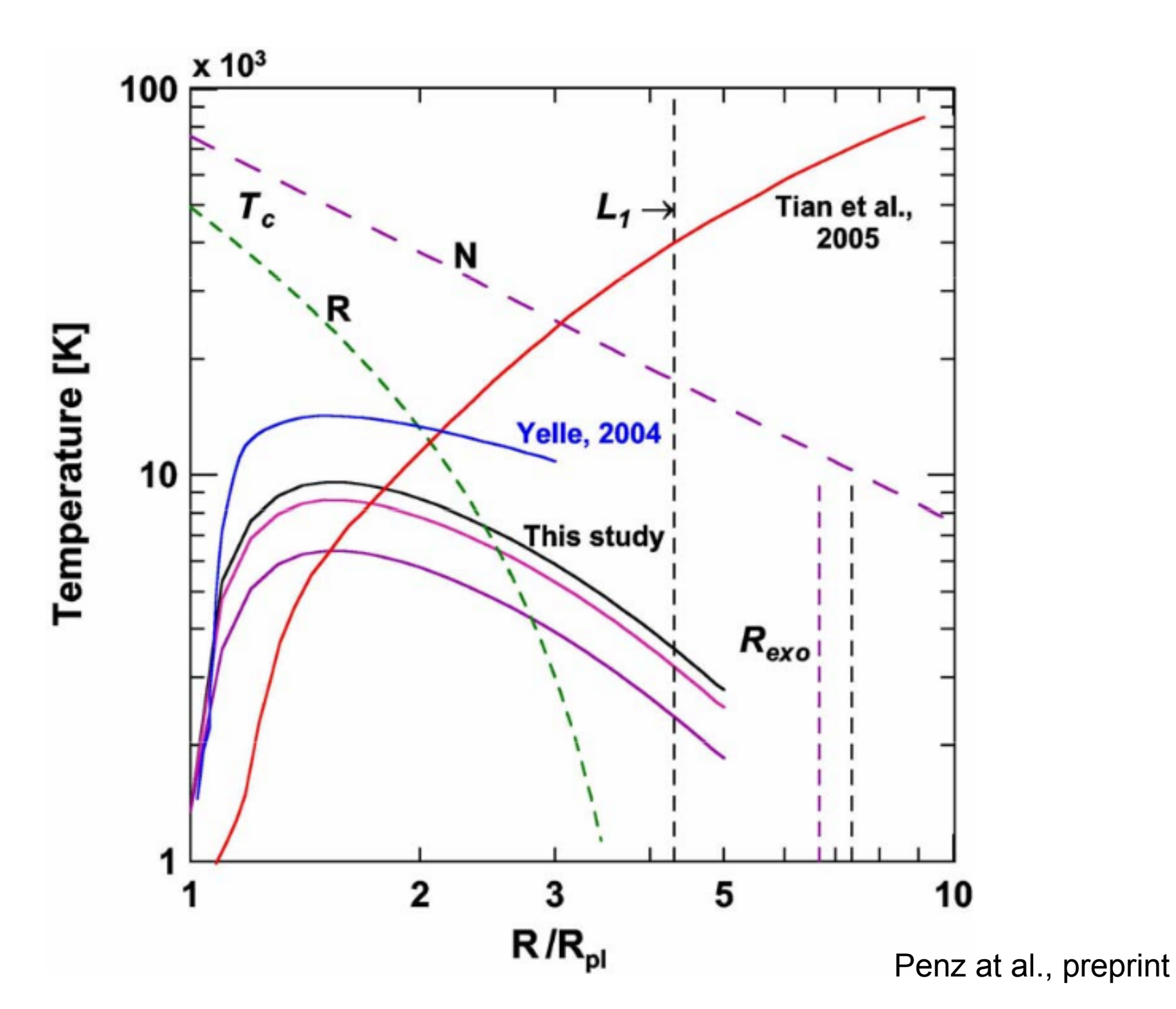
**Table .1.** Default physical parameter values used in the simulations, unless otherwise noted.

Name	Symbol	Value
Exobase radius	$R_0$	2 · 108m
Exobase temperature		$10^{4}$ K
Exobase density		$10^{14} \mathrm{m}^{-3}$
H-H crossection		$10^{-21}$ m <sup>2</sup>
H-H+ crossection		$2 \cdot 10^{-19} \text{m}^2$
UV absorption rate	$\tau_{\rm r}$	$0.7s^{-1}$
Photoionization rate	$\tau_{i}$	$7 \cdot 10^{-5} s^{-1}$
Obstacle standoff distance	$X_0$	$2.3 \cdot 10^{8}$ m
Angular velocity	ω	$2 \cdot 10^{-5} \text{rad/s}$
Solar wind density		$2 \cdot 10^{9} \text{m}^{-3}$
Solar wind velocity	$u_{\rm sw}$	$10^{5} \text{m/s}$
Solar wind temperature	$T_{\mathrm{sw}}$	$1.2 \cdot 10^5 \text{K}$

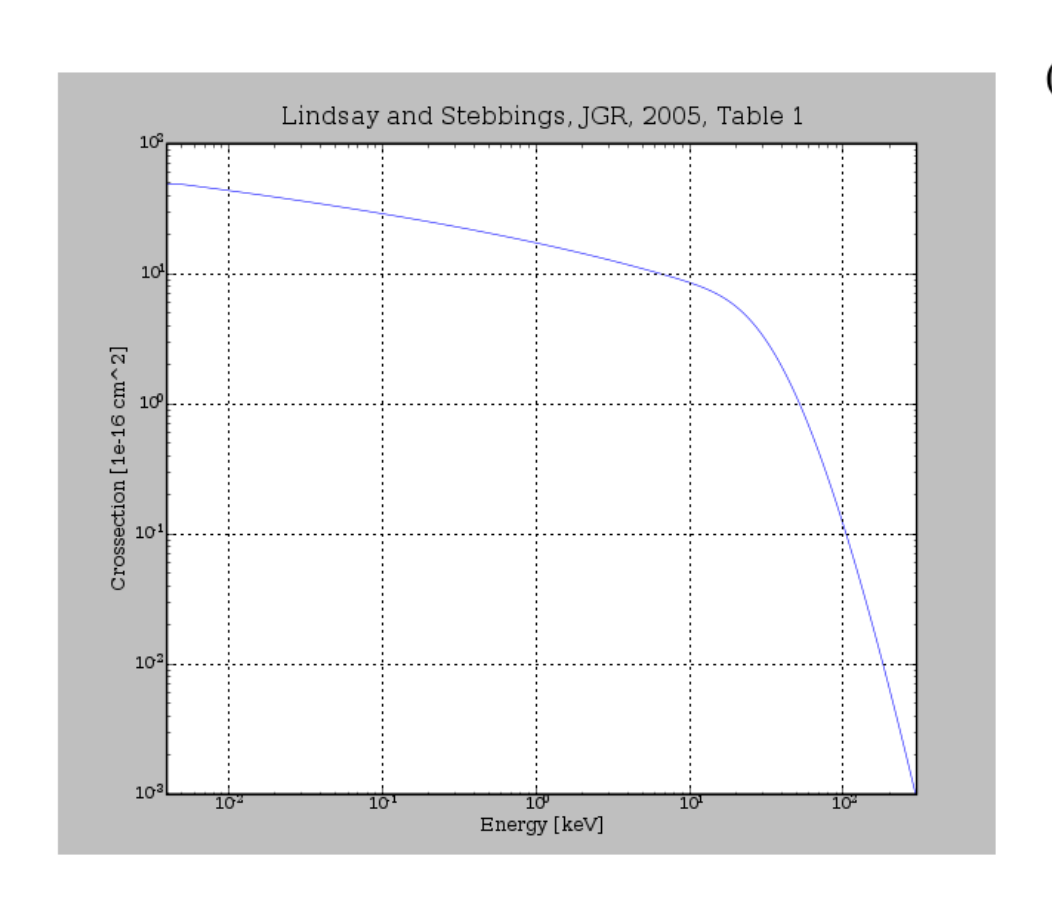
**Table .2.** Default numerical parameter values used in the simulations, unless otherwise noted.

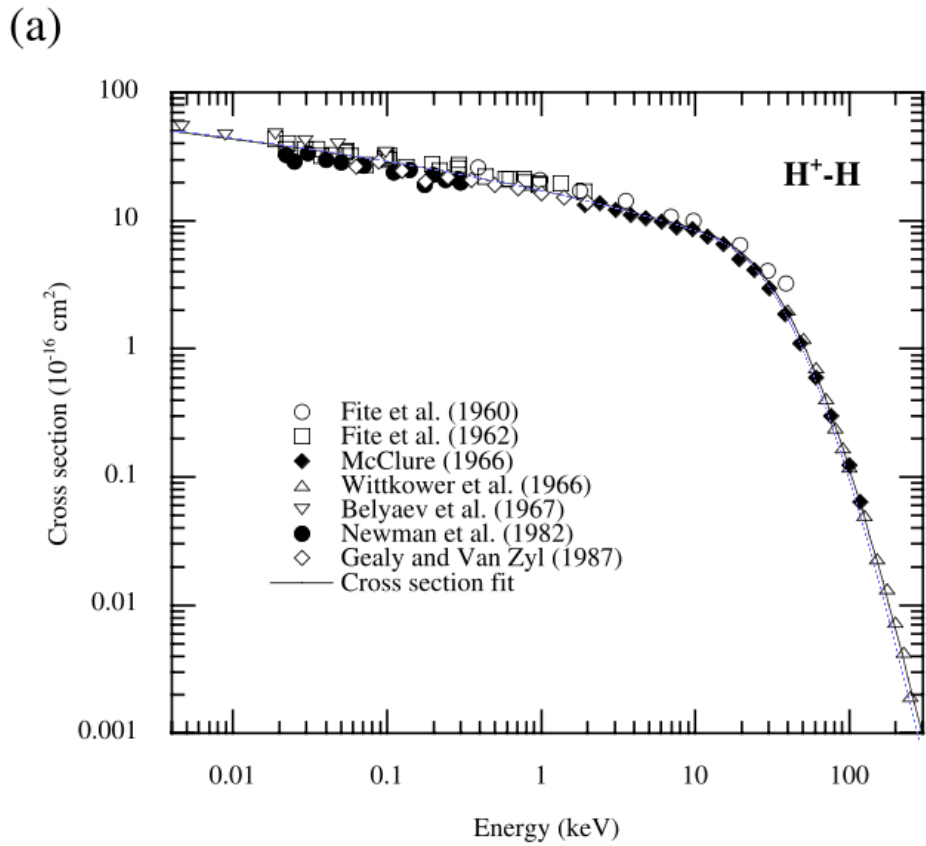
Name	Symbol	Value
	$x_{\min}$	−5 · 10 <sup>9</sup> m
	$x_{\max}$	$2 \cdot 10^9 \text{m}$
	$y_{\min}$	$-7 \cdot 10^{9}$ m
	$y_{\text{max}}$	$7 \cdot 10^{9} \text{m}$
	$z_{\min}$	$-3.5 \cdot 10^{9}$ m
	$z_{\rm max}$	$3.5 \cdot 10^{9}$ m
Number of cells		$16 \cdot 10^{6}$
Final time	$t_{ m max}$	$10^{5}$ s

Stellar wind velocity and temperature  $u_{sw} = 100 \text{ km/s}, T_{sw} = 1.2 \cdot 10^5 \text{ K}$ 

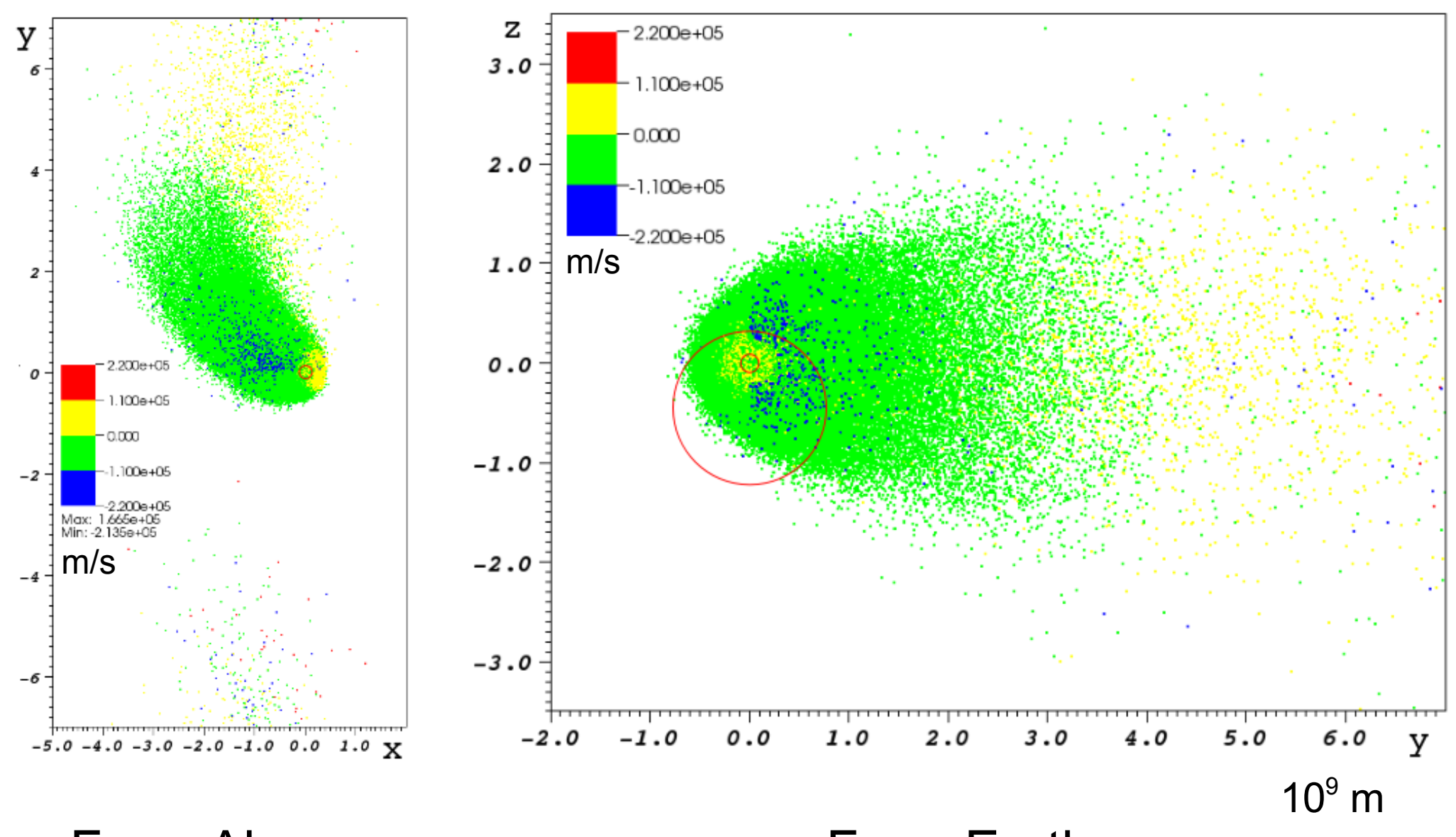


# Charge exchange cross sections





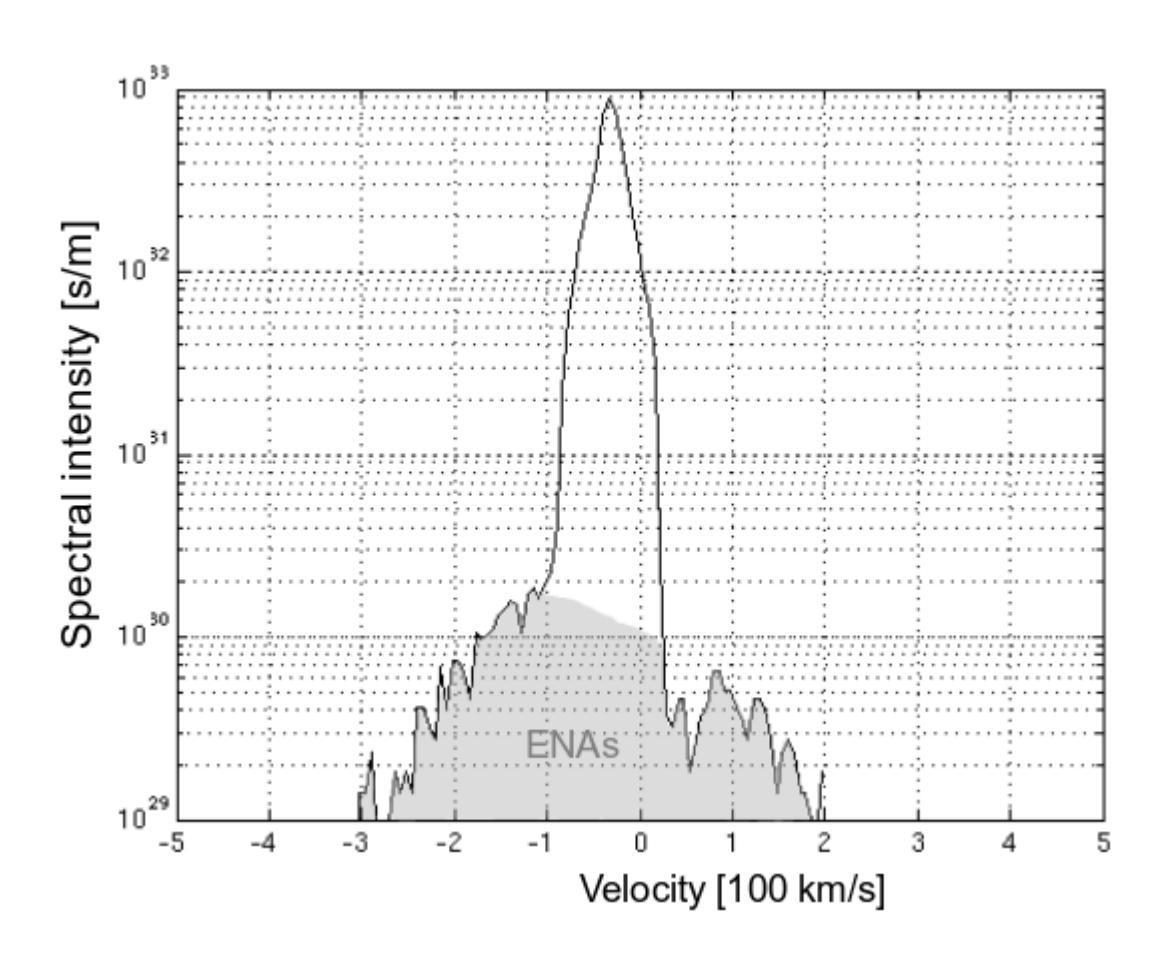
## x-axis velocity of H



From Above

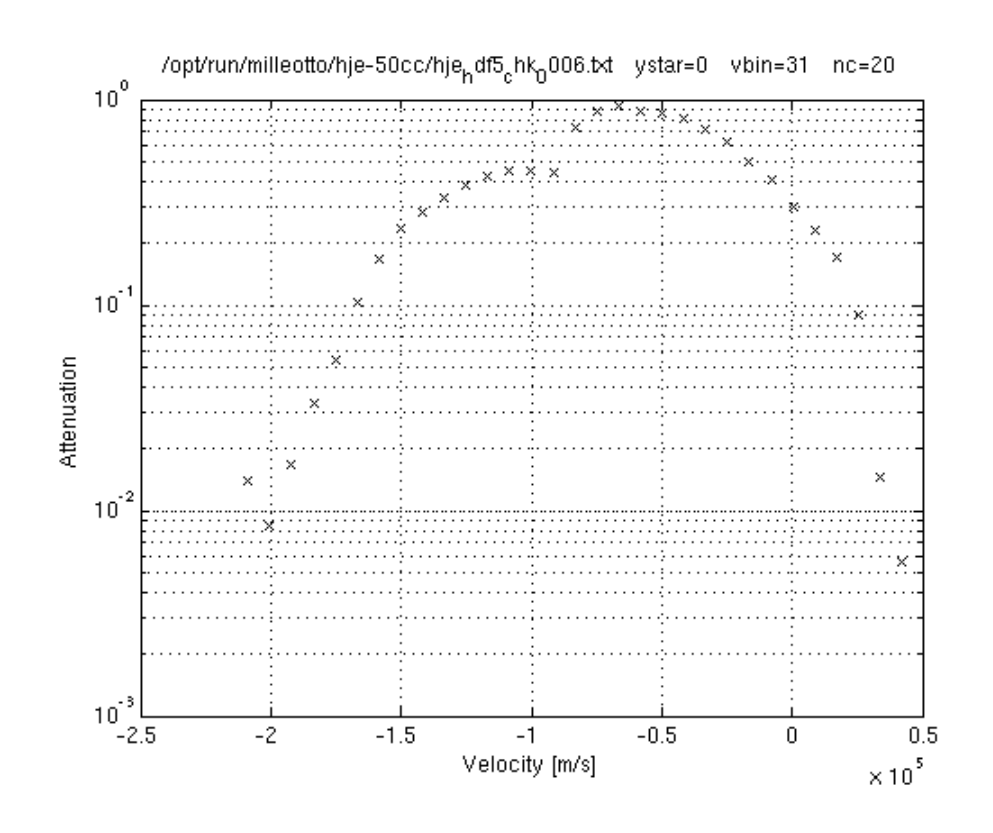
From Earth

## Average H Velocity Spectrum (along *x*-axis)



#### **Attenuation**

- Columns along x-axis in a grid in front of the star
- Attenuation spectrum computed for each column
- Average attenuation for each velocity is computed
- This attenuation can then be applied to the out-of-transit observed spectrum, and compared to the in-transit spectrum



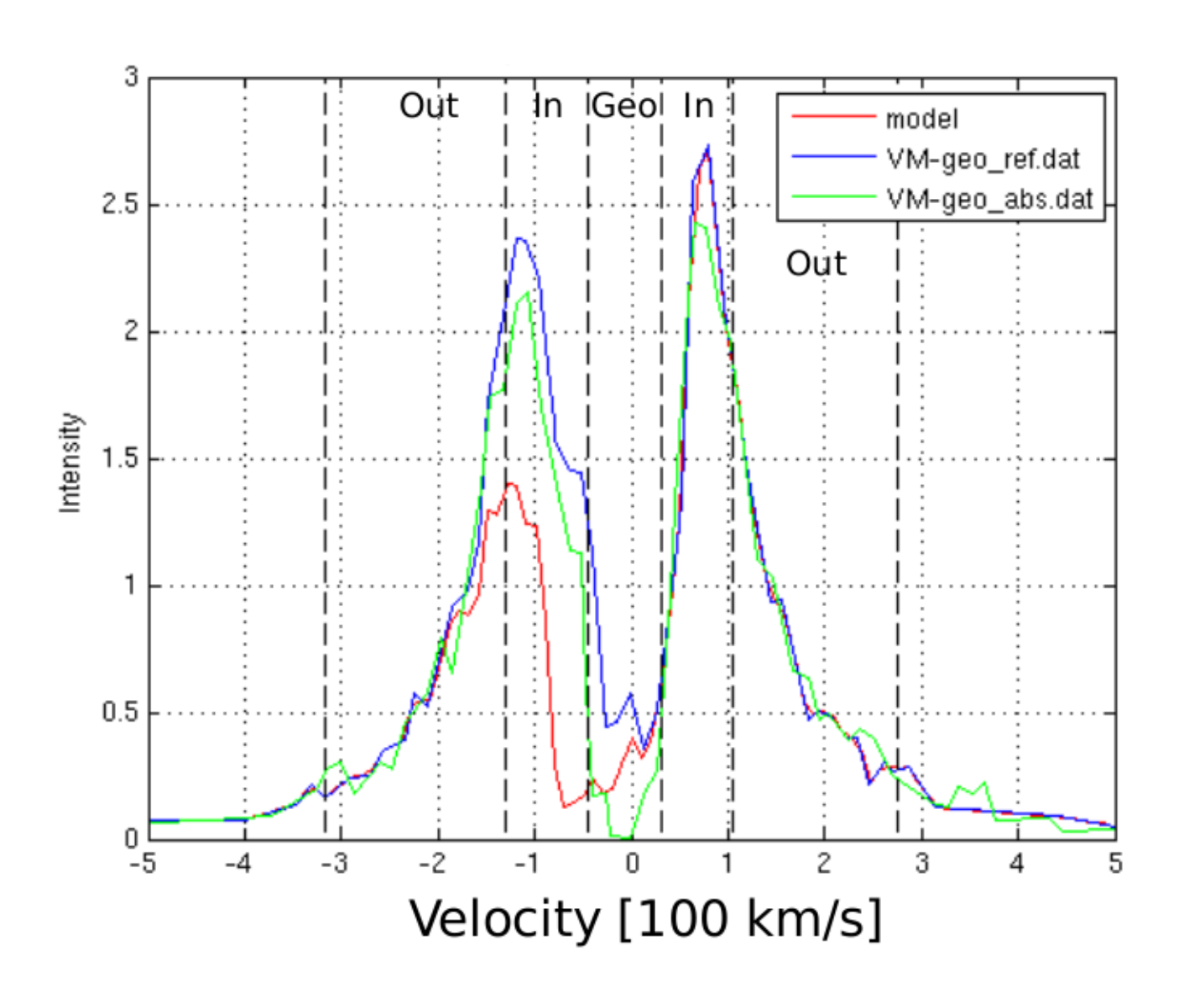
#### Lyman-alpha attenuation

Given the positions of all the hydrogen meta particles at a certain time, we now proceed to compute how they attenuate the stellar Lyman-alpha radiation. We discretize the yz-plane using a grid. For each cell in the grid we compute the velocity spectrum of all hydrogen atoms in the column along the x-axis corresponding to the cell. We then subtract 13 km/s from the x-axis velocity of all atoms to account for the velocity of the star toward the Sun. This velocity spectrum can be converted into a frequency spectrum using the relation  $f = f_0 + v/\lambda_0$ , where v is the velocity,  $\lambda_0 = 1215.67 \cdot 10^{-8}$  cm, and  $f_0 = c/\lambda_0$ . This spectrum, h(f), is normalized to have unit integral. Assuming only single scattering, the attenuation factor at each frequency is then

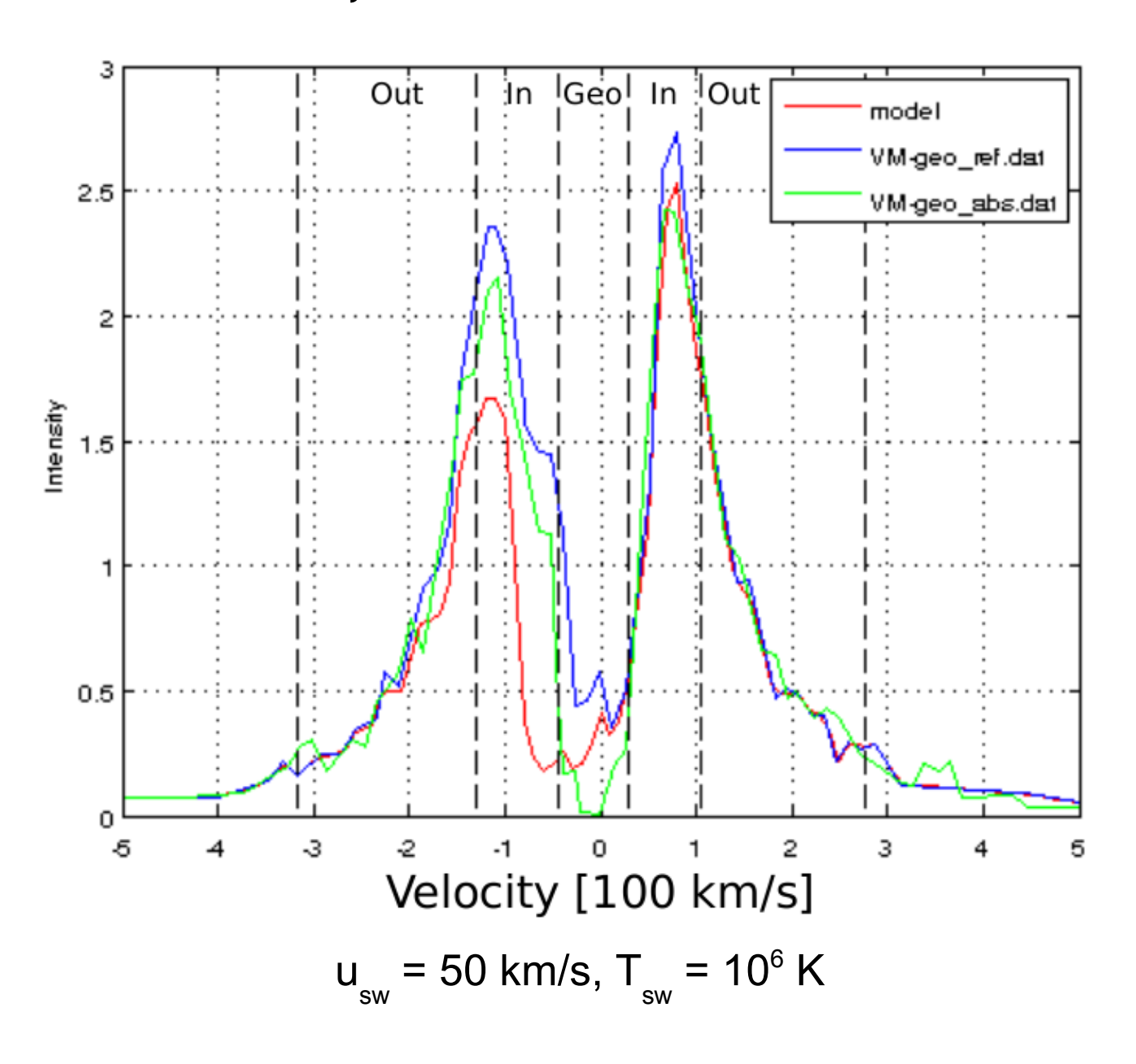
$$1 - e^{-ngah(f)}$$
,

where n is the column density,  $g = 2 \cdot 0.4162$ , and a = 0.026 Hz cm<sup>2</sup>. This attenuation factor is then averaged over all columns in the yz-grid, except those whose center fall outside the projected limb of the star, or inside the planet disc. The computed attenuation is shown in Fig. 2, where we see that the separation between ENAs and exospheric hydrogen that was visible in the velocity spectrum also is apparent in the attenuation spectrum. This attenuation is then applied to the observed spectrum. At each velocity we simply multiply the observed spectrum by the attenuation factor.

# Comparison with Observation



# Slow, Hot Stellar Wind



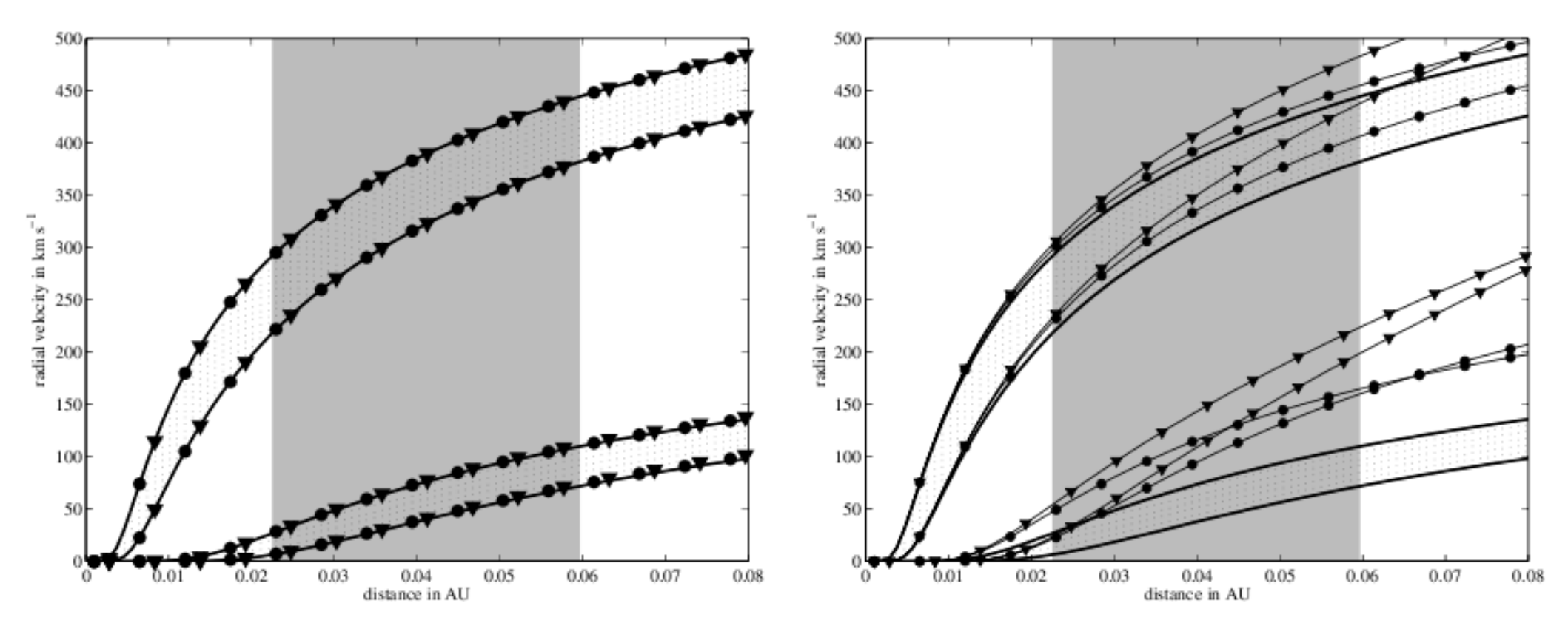
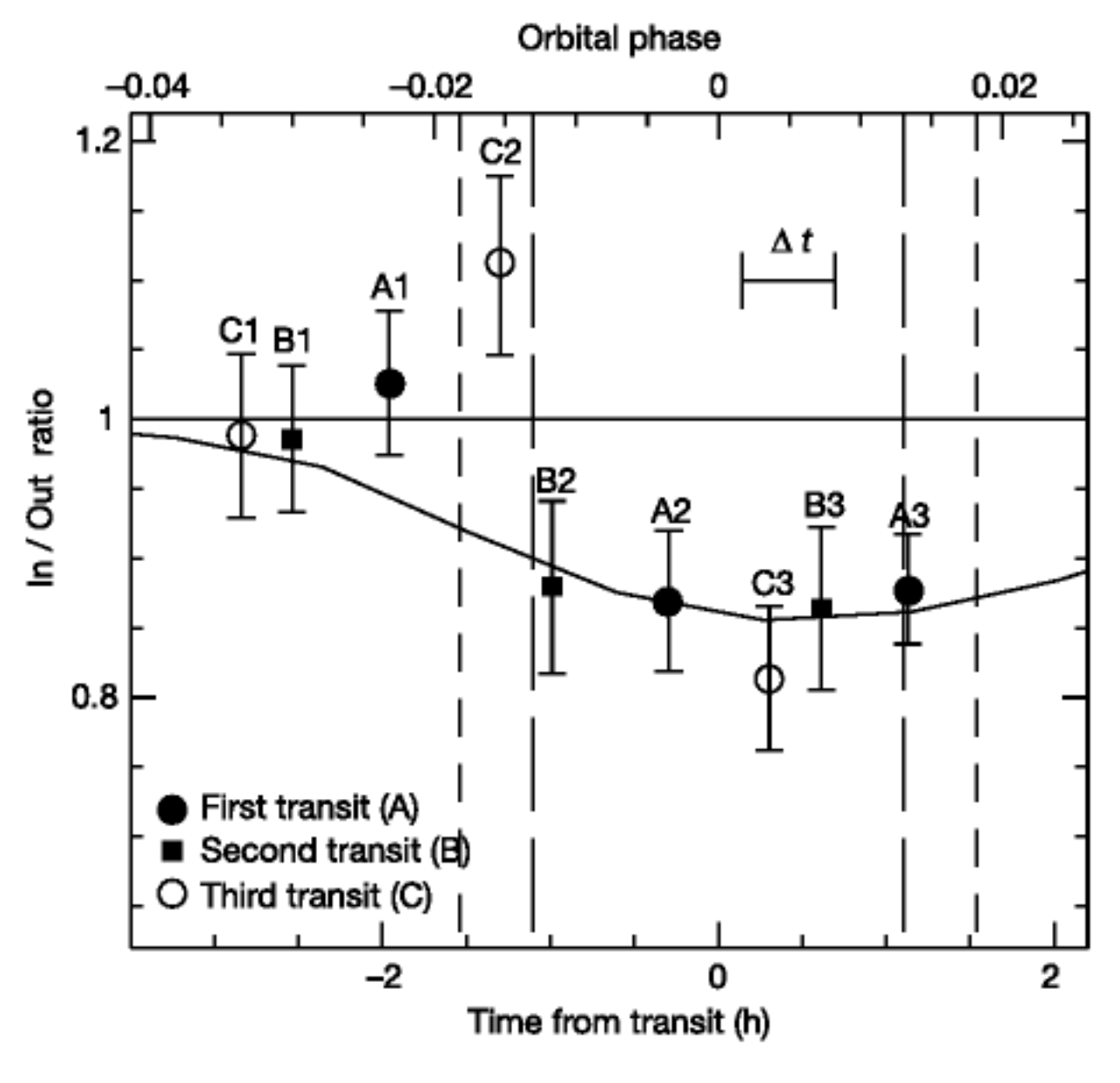


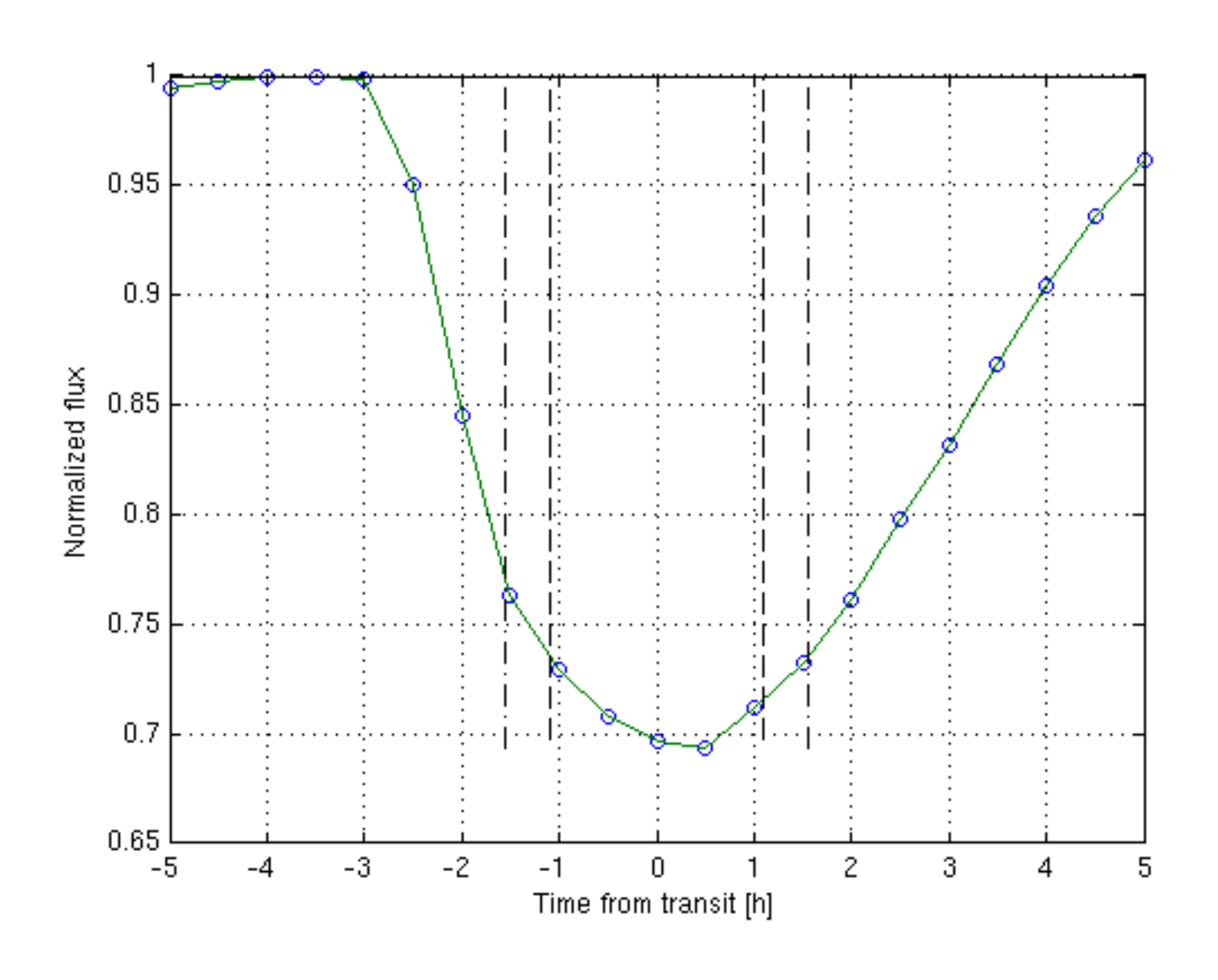
Fig. 2. Radial velocity profiles for v And and HD 46375 calculated with the Weber & Davis model. The results are compared with the Parker limits for all stars listed in Table 3 which are indicated by the dotted patches. The left panel shows the changes due to inclusion of a rotation period of 30 d and the right one for 3 d. Again, the upper velocity profiles belong to  $T = 2.0 \cdot 10^6$  K and and the lower to  $T = 0.5 \cdot 10^6$  K. The magnetic field at the base of the corona was set to  $1 \cdot 10^{-4}$  T (dots) and  $10 \cdot 10^{-4}$  T (triangles). For slow rotation, hardly any differences at all are observed with respect to the Parker limit solutions. For the faster rotation, the velocity changes significantly. These changes are larger for the lower temperature as well as for the star with the bigger mass and radius (v And) which yields the slower velocity. The grey patch indicates the spatial distribution of the planetary orbits.



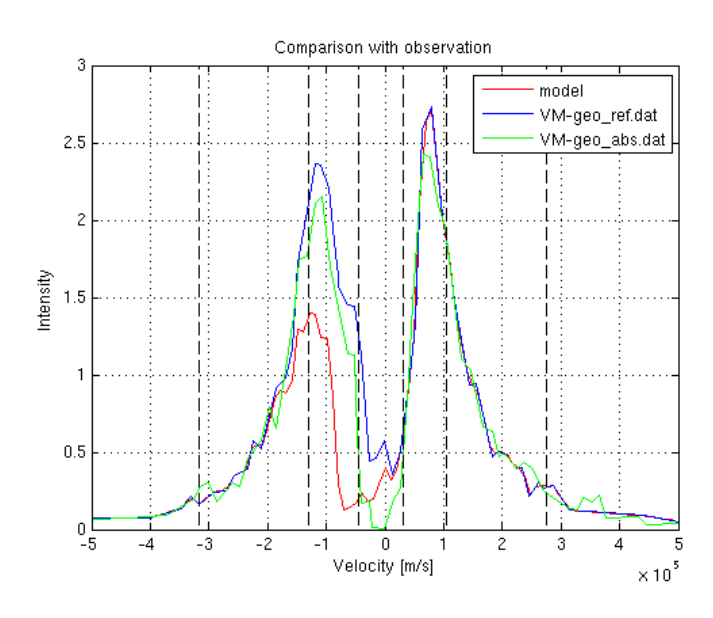
**Figure 3** Relative flux of Lyman  $\alpha$  as a function of the HD209458's system phase. The averaged ratio of the flux is measured in the ln (1,215.15–1,215.50 Å and 1,215.80–1,216.10 Å) and the Out (1,214.40–1,215.15 Å and 1,216.10–1,216.80 Å) domains in individual exposures of the three observed transits of HD209458b.

Vidal-Madjar, Nature, 422, 2003

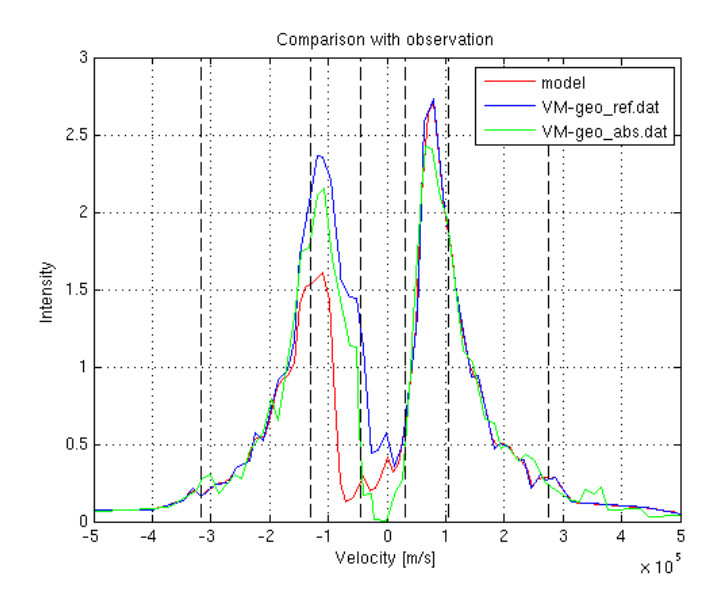
# Flux Change During Transit



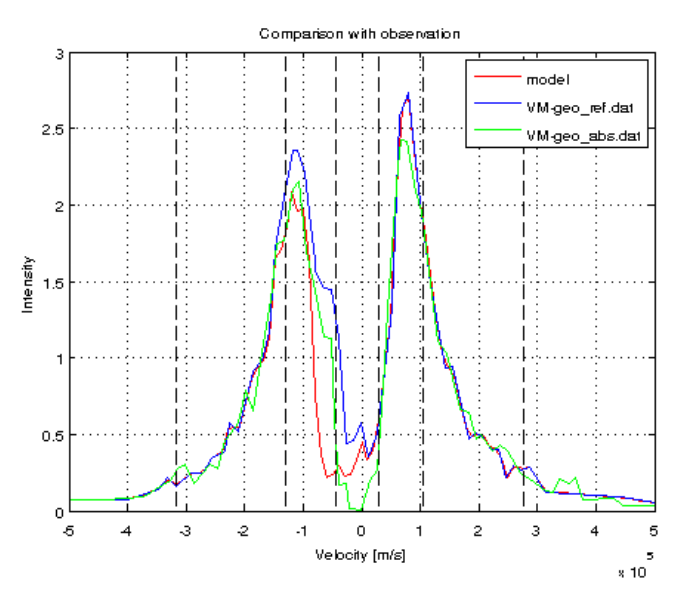
#### Attenuation spectra when parameter values changes



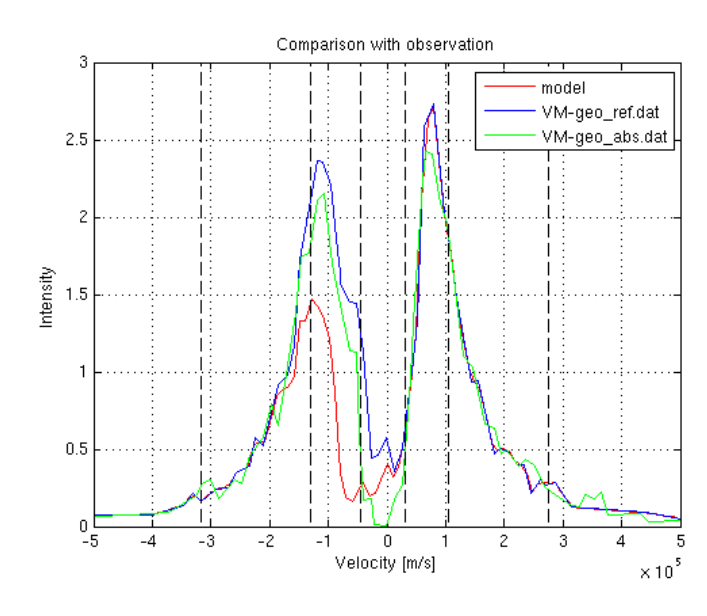
Default parameter values



Solar wind density 1000 cm-3 (instead of the default 2000 cm-3)

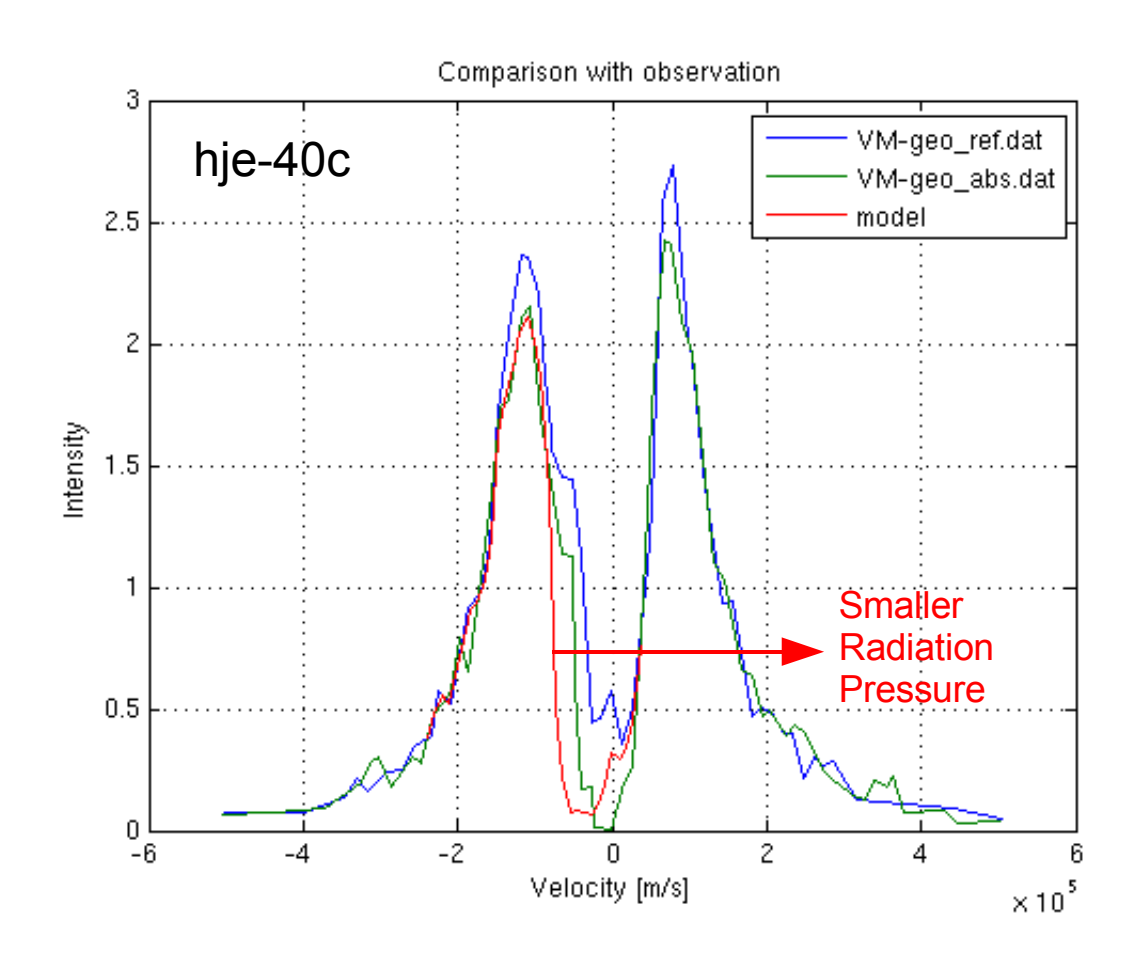


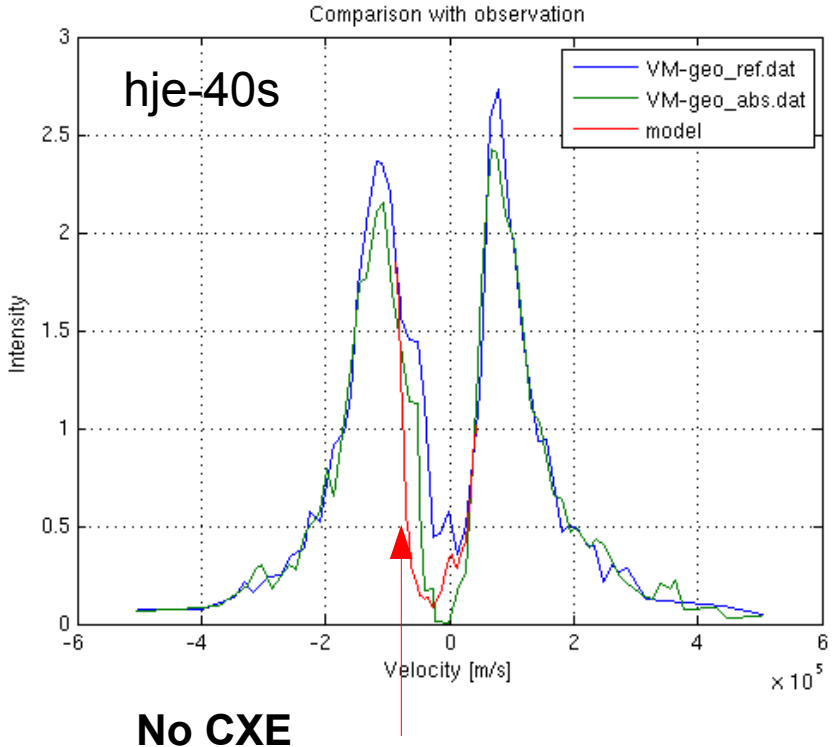
Exobase temperature of 7000 K (instead of the default 10000 K)



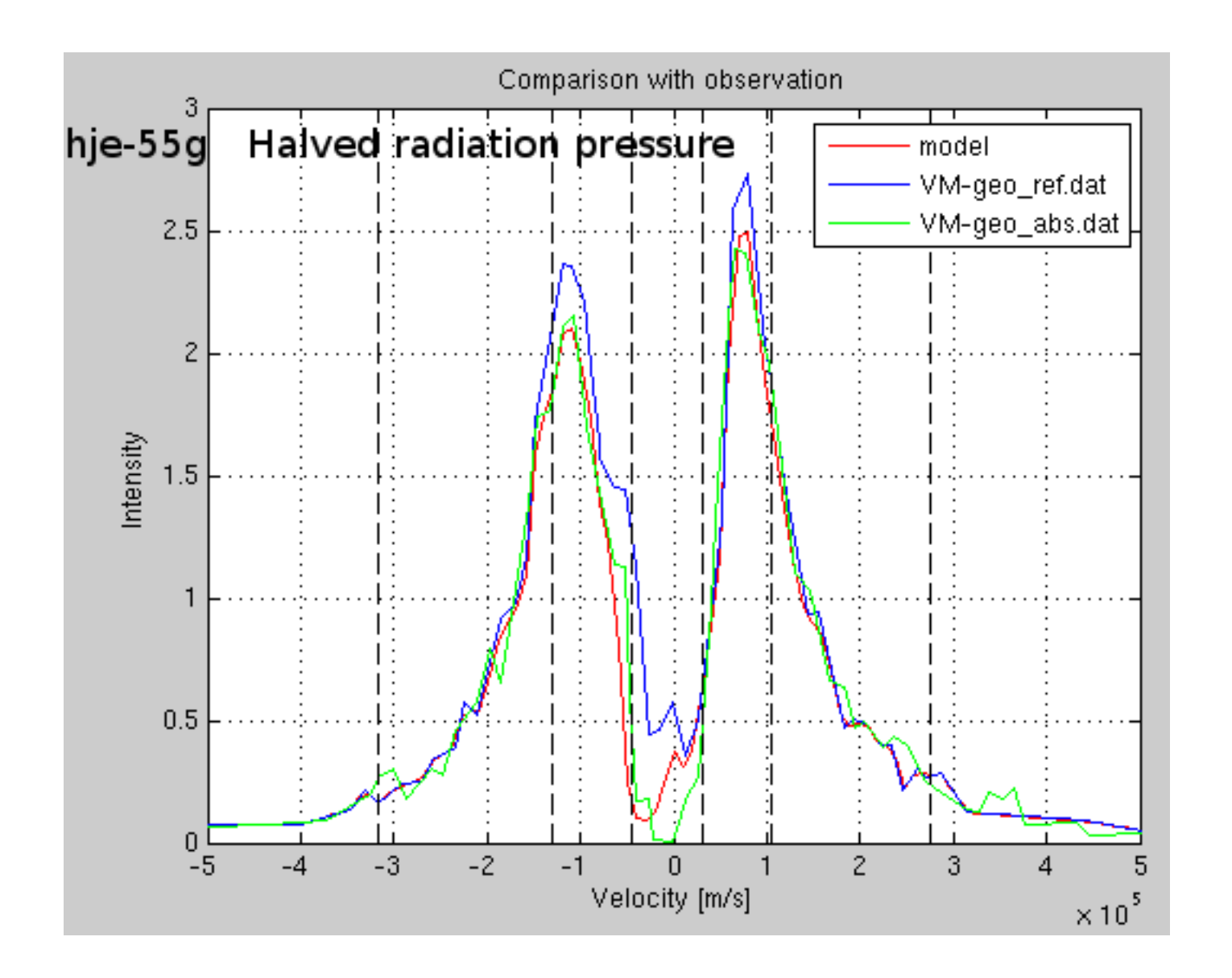
Exobase density of 0.8e14 m-3 (instead of the default 1e14 m-3)

# Parameter effects on spectrum

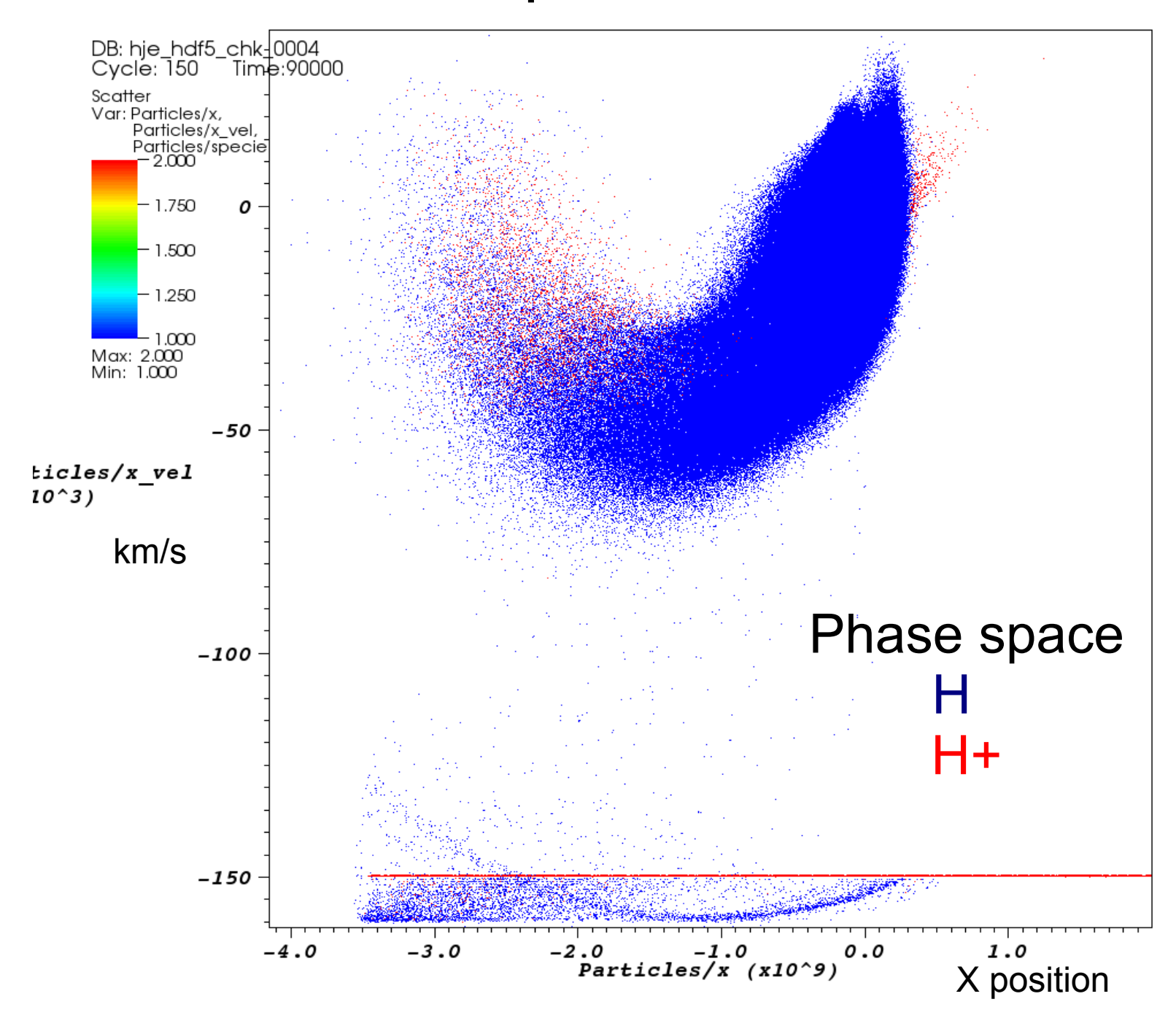




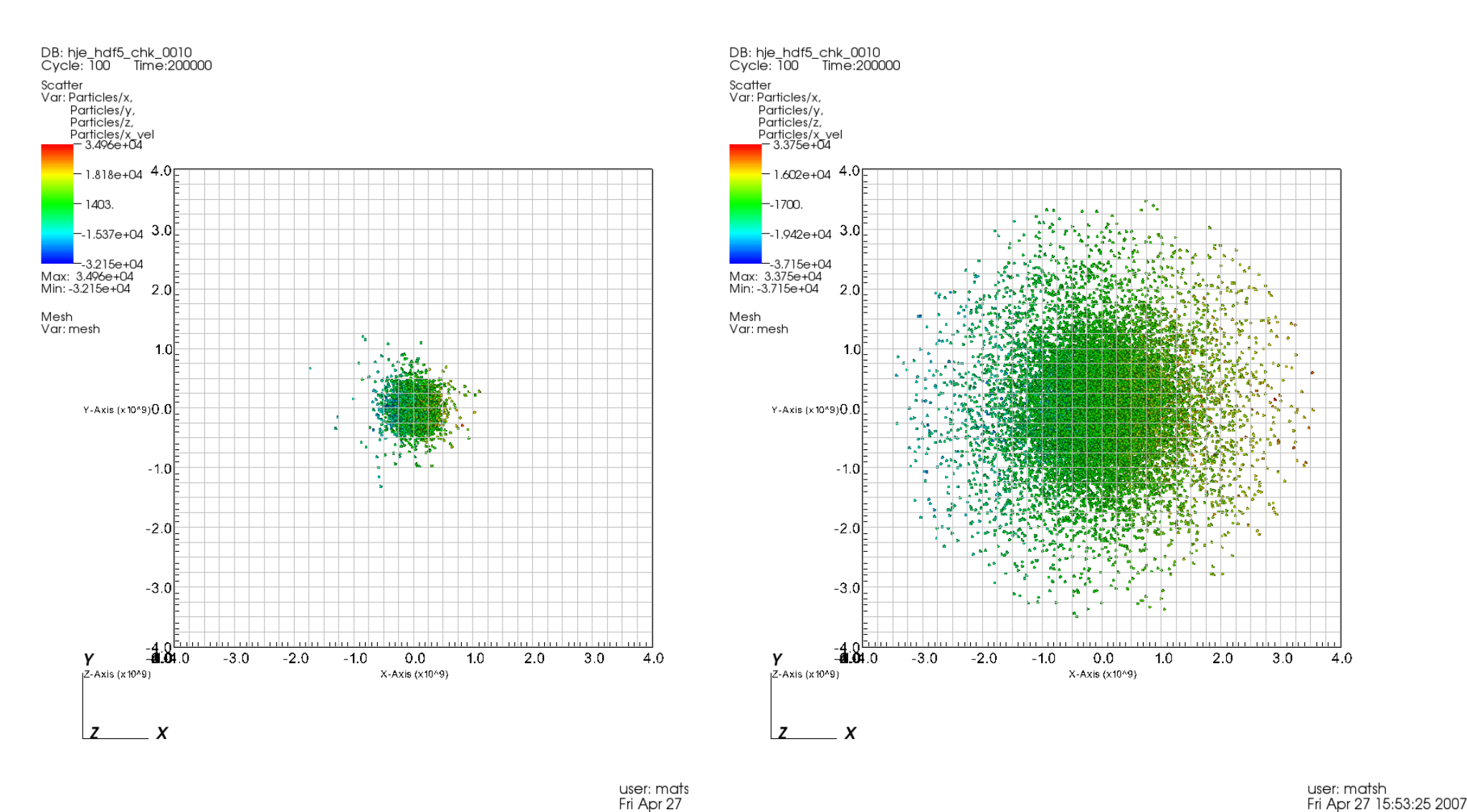
=> cutoff at too low velocity, even with high radp.
The "walls" of the hole are too steep to ever explain the observation (in this model), no matter what the parameters!



## Phase space X - Xvel



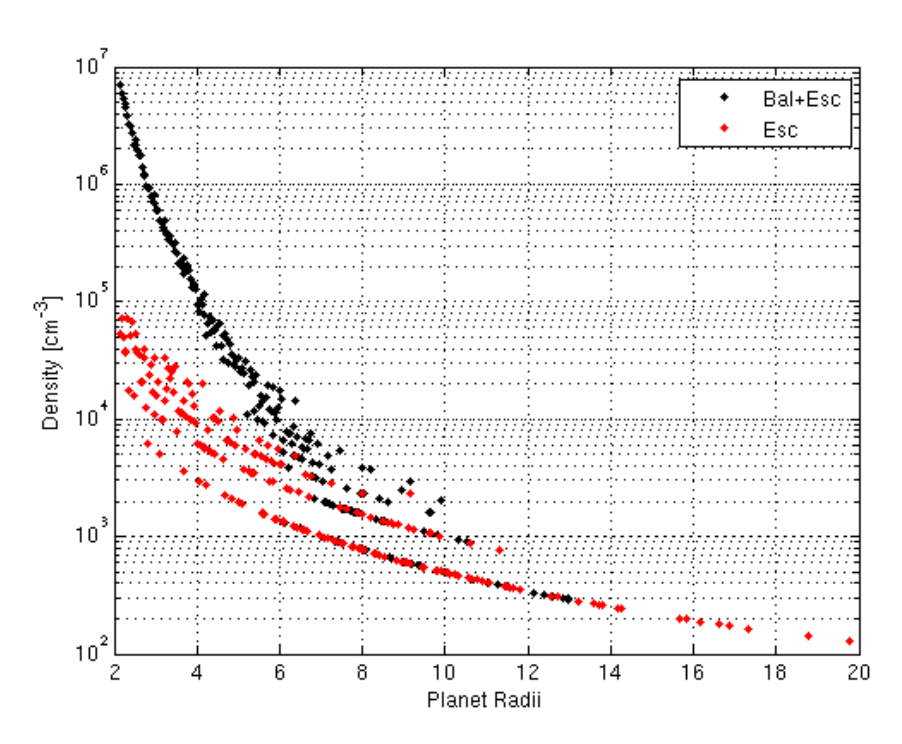
#### Photoionization greatly reduces the exosphere



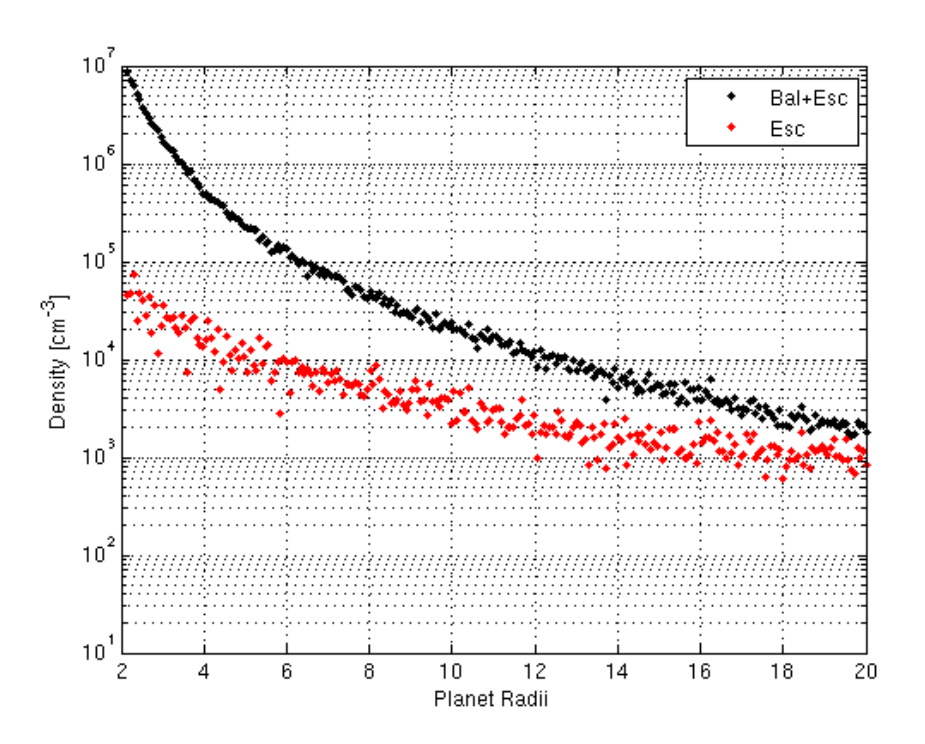
Photoionization - rate 7e-5

No Photoionization

#### Density profiles



Photoionization - rate 7e-5

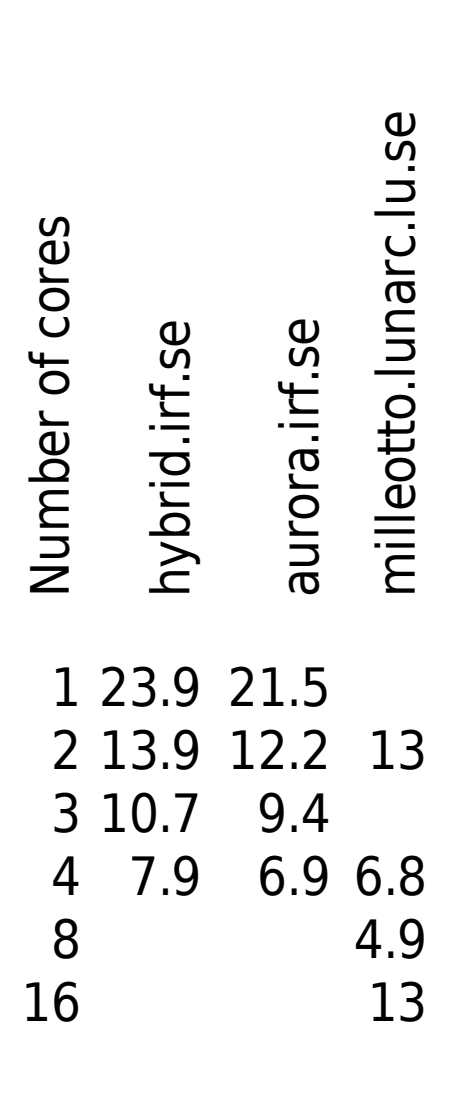


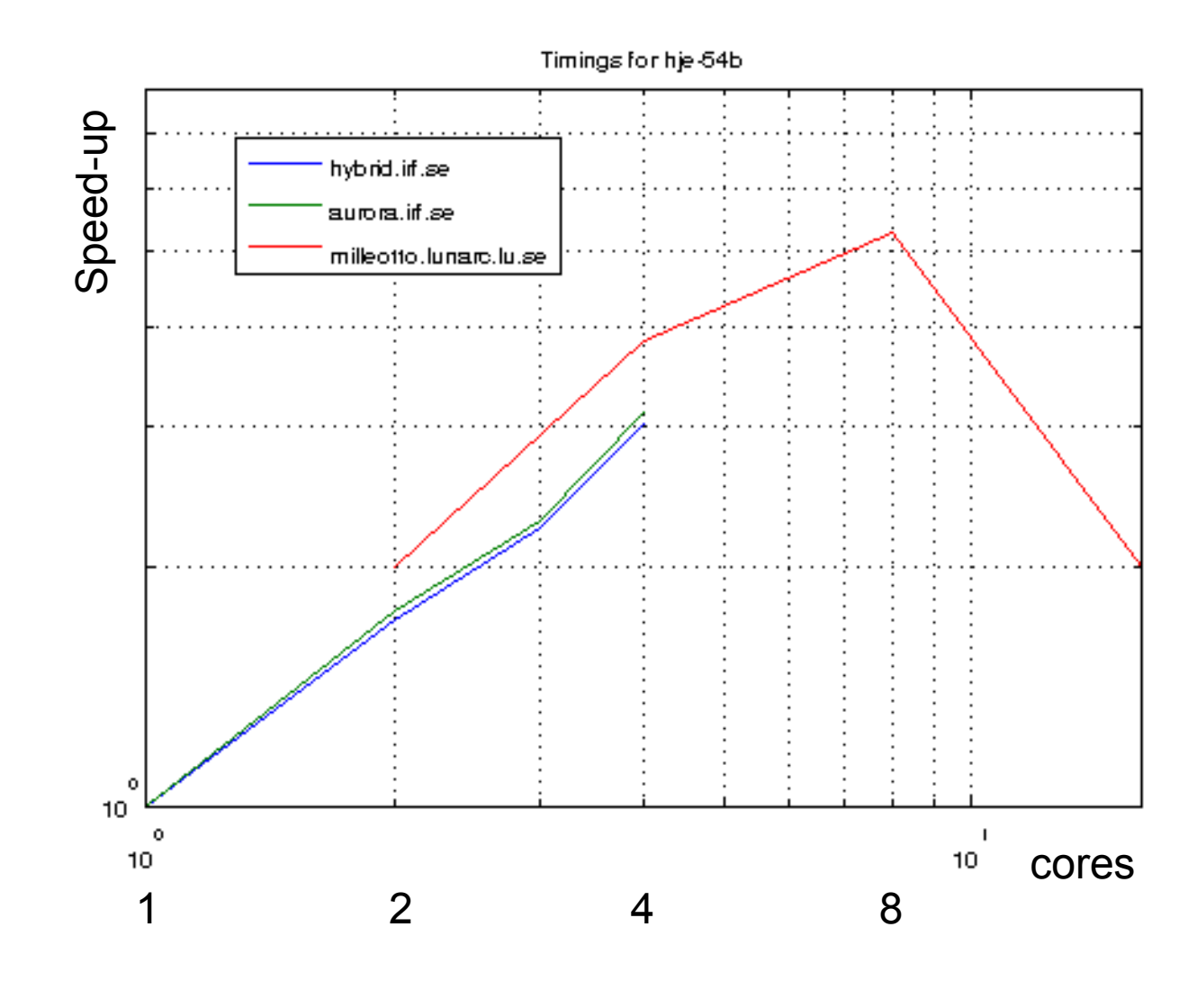
No Photoionization

#### Software

We use an existing software, Flash, developed at the University of Chicago <sup>6</sup>, that provide adaptive grids and is fully parallelized, and that we have extended to do DSMC modeling of planetary exospheres Flash is a general parallel solver for compressible flow problems. It is written in Fortran 90, well structured into modules, and open source. The parallelization is to a large extent handled by the Paramesh<sup>7</sup> library that implements a block-structured adaptive cartesian grid with the Message-Passing Interface (MPI) library as the underlying communication layer.

# Computational Details





## Conclusions

- Energetic Neutral Atoms (ENAs) can explain the observed Lyman  $\alpha$  absorption
- Stellar wind properties can be inferred from Lyman  $\alpha$  observations through ENAs
- The stellar wind depletion from charge-exchange has to be accounted for in models

